baumannii, and GIM-1 from *P. aeruginosa* (*27*) are encoded by mobile genes on a plasmid. So far, the three-dimensional structures of the subclass B1 metallo-β-lactamases have been solved for BcII (*7*, *28–30*), BlaB (*31*), CcrA (*32–34*), IMP-1 (*35*, *36*), VIM-2 (*37*, *38*) and SPM-1 (*10*).

In 1999, the chromosome-encoded *C. indologenes* metallo-β-lactamase IND-1 was first isolated (*24*), and six IND variants, designated IND-2 to IND-6 and IND-2a, have been detected to date (*39–41*). *Chryseobacterium indologenes* are aetiological agents of infection associated with the use of indwelling devices (*42*). The amino acid sequences of the above-mentioned six IND variants share 72–92% identity with that of IND-1 (Fig. 1). Of these enzymes, kinetic parameters are available for IND-1, IND-2, IND-5 and IND-6, though in the case of IND-1, only a comparison of the K_m values is available (*24*, *39–41*).

In 2005, Arakawa *et al.* isolated a chromosomal metallo-β-lactamase produced by a *C. indologenes* clinical isolate from the urinary tract infection of a patient in Japan (MRY040066 strain). Based on a comparison of the amino acid sequence of metallo-β-lactamase from *C. indologenes* MRY040066 (denoted as IND-7) with that of IND-1, IND-7 identified most with IND-1 (99%) where an isoleucine at position 90(72) in IND-1 was replaced by a valine in IND-7. (In this paper, the amino acid residues are designated by a BBL numbering (*4*), and the amino acid sequence number from the N-terminus for mature protein—the latter is in parenthesis.)

The aim of this study is to fully characterize the three-dimensional structure of IND-7 from *C. indologenes*, because the X-ray crystal structures of IND variants are not available. We report here the crystal structure of metallo-β-lactamase IND-7 at a resolution of 1.65 Å.

Materials and Methods

Cloning

The bla_{IND-7} gene was amplified with the primers IND-F (5′-CAT ATG AAA AAA AGC ATC CGT TTT-3′), which have an NdeI linker (underlined), and IND-R (5′-GGA TCC CTA TTT TTT ATT CAG AAG TT-3′), which have a BamHI linker (underlined), using an Expand High-Fidelity PCR system (Roche). The template DNA was extracted from the clinically isolated *C. indologenes* strain MRY040066. The amplicon was ligated with a pGEM-T vector (Promega), and was partially excised by digestion with NdeI and BamHI. The excised fragment was subcloned into the expression vector pET29a(+) (Novagen) to yield plasmid pET29a(+)/bla_{IND-7}.

Expression and purification

A 25-ml overnight preculture of *Escherichia coli* BL21(DE3), which was transformed by plasmid pET29a(+)/bla_{IND-7}, was used to inoculate 10 l of LB broth supplemented with 50 μg/ml kanamycin, and the resulting culture was grown at 37°C with shaking until the culture reached an OD_{600} of about 1.0. The culture was developed in 0.1 mM isopropyl-β-D-thiogalactopyranoside (IPTG) and shaken at 37°C for 2 h. The culture was centrifuged at 5,000 *g* for 10 min at 4°C. The pellets (about 40 g, wet weight) were washed by resuspension in 40 ml of 20 mM Tris–HCl pH 7.4, with repeat centrifugation. The pellets were resuspended in 40 ml of the same buffer, disrupted by sonication for 5 min and centrifuged at 100,000 *g* for 75 min at 4°C. After removal of insoluble components by filtration (MILLEX-GP 0.45 μm, Millipore), the filtrate was loaded into an SP Sepharose Fast Flow column (φ 2.6 × 10 cm, GE Healthcare) pre-equilibrated with 20 mM Tris–HCl pH 7.4, and the proteins were eluted with a linear gradient of 0–0.5 M NaCl. Fractions were analysed by sodium dodecyl sulphate polyacrylamide gel electrophoresis (SDS-PAGE) and by their ability to turn over nitrocefin as a substrate. Fractions containing the desired activity were pooled and concentrated to a volume of 10 ml by Ultracel YM-10 (Millipore). The concentrated protein was loaded into a Sepharose G-75 column (φ 1.6 × 10 cm, GE Healthcare) and was eluted with 20 mM Tris–HCl pH 7.4 containing 0.3 M NaCl. Fractions containing the IND-7 protein were pooled and concentrated to a volume of 6 ml. The protein was then reloaded into a Sephacryl HR-100 column (φ 1.6 × 10 cm, GE Healthcare) and was eluted with 20 mM Tris–HCl pH 7.4 containing 0.3 M NaCl. The protein was further concentrated to 14 mg/ml using both Ultracel YM-10 (Millipore) and Amicon Ultra-15 (Millipore). The purity of the IND-7 protein was estimated to be greater than 95% by SDS-PAGE at a protein concentration of 1 mg/ml. Prior to the X-ray diffraction experiments, a buffer solution of the IND-7 protein was converted from 20 mM Tris–HCl containing 0.3 M NaCl to 20 mM HEPES–NaOH pH 7.5. For crystallization, the purified IND-7 protein was concentrated to about 14 mg/ml using both Amicon YM-10 (Millipore) and Amicon Ultra (Millipore).

Crystallization

Screening for IND-7 crystallization conditions was performed at 20°C by the hanging-drop method using Crystal Screen and Crystal Screen II kits (Hampton Research): drops mixed 2 μl of a protein solution with 2 μl of a reservoir solution. The best crystals suitable for X-ray diffraction study were obtained from condition No. 17 using the Crystal Screen kit [30%(w/v) PEG4000, 0.1 M Tris–HCl pH 8.5 and 0.2 M Lithium sulphate monohydrate], which grew as plates within 3 months at 20°C.

Data collection and refinement

All diffraction data were collected at 100 K after cryoprotection by a brief exposure to a reservoir solution containing 30% (w/v) PEG4000 at the SPring-8 (Harima, Japan) and the Photon Factory (Tsukuba, Japan). The data set used the structural analysis that was collected at the SPring-8 on a beamline 38B1 (Harima, Japan) at a resolution of 1.65 Å and a wavelength of λ = 1.00 Å. Data for the crystal were integrated, merged, and scaled using HKL-2000 (*43*). The refined structure (PDB code: 1M2X) of BlaB from *C. meningosepticum* at a 1.5 Å resolution (*31*) was used as the search model for molecular replacement using the AMoRe (*44*) and Molrep (*45*) software programs, which are a component of the CCP4 program suite v.6.0.0 (*46*). The interactive graphics programs O (*47*) and Coot v.0.1.2 (*48*) were used to build the IND-7 structure (*47*). The refinement was performed with the CNS (*49*) and Refmac (*50*) software programs. Data collection and refinement statistics are listed in Table I. Selected bond distances and angles are shown in Table II.

PDB Accession Code

The atomic coordinates and structure factors have been deposited in the Protein Data Bank under accession code 3L6N.

Nucleotide Sequence Accession Number

The nucleotide sequence encoding IND-7 characterized in this study appears in the EMBL/GenBank/DDBJ databases under accession AB529520.

Results and Discussion

Overall structure of IND-7

The structure of IND-7 from *C. indologenes* was solved by molecular replacement. The final refined structural model contained residues Gln38(21)–Lys293(238), two zinc(II) ions (Zn1 and Zn2), two sulphate ions, and 327 ordered water molecules per asymmetric unit, and was refined to $R_{working} = 17.7\%$ and $R_{free} = 20.0\%$ at 1.65 Å resolution (Table I). The root mean square differences (RMSD) from the ideal

```
BBL No.      20        30        40        50        60        70        80        90
             |         |         |         |         |         |         |         |
IND-1       MKKSIRFFIVSILLSPFASAQVKDFVIEPPIKNNLHIYKTFGVFGGK-EYSANSMYLVTKKGVVLFDVPWEKIQYQSL  77
IND-2       MKKSIQLLMMSMFLSPLINAQVKDFVIEPPVKPNLYLYKSFGVFGGK-EYSANAVYLTTKKGVVLFDVPWQKEQYQTL  77
IND-2a      MKKSIQLLMMSMFLSPLINAQVKDFVIEPPVKPNLYLYKSFGVFGGK-EYSANAVYLTTKKGVVLFDVPWQKEQYQTL  77
IND-3       MKKRIQFFMVSMMLSSLFSAQVKDFVIEPPIKKNLHIYKTFGVFGGK-EYSANSVYLVTQKGVVLFDVPWEKVQYQSL  77
IND-4      MRKNVRIFTVLSLFLINFFNAQARDFVIEQPFGKQLYLYKTFGVFDGK-EYSTNALYLVTKKGVVLFDVPWQKTQYQSL  78
IND-5       MKKRIQFFMVSMMLAPMFNAQVKDFVIEPPIKNNLHIYKTFGVFGGK-EYSANSVYLVTKKGVVLFDVPWEKAQYQSL  77
IND-6       MKRRIQFFMVSMMLTPLFSAQVKDFVIEPPIKKNLYIYKTFGVFGGK-EYSANSVYLVTKTGVVLFDVPWEKAQYQSL  77
IND-7       MKKSIRFFIVSILLSPFASAQVKDFVIEPPIKNNLHIYKTFGVFGGK-EYSANSMYLVTKKGVVLFDVPWEKVQYQSL  77
               : :  :  :: : :::                                   :                  :

BBL No.       100       110       120       130       140       150       160       170
               |         |         |         |         |         |         |         |
IND-1       MDTIK-KRHNL-PVVAVFATHSHDDRAGDLSFFNNK-GIKTYATAKTNEFLKKDG----------------KATSTEIIK  138
IND-2       MDTIQ-KRHHL-PVIAVFATHSHDDRAGDLSFYNQK-GIKTYATAKTNELLKKDG----------------KATSTEIIK  138
IND-2a      MDTIQ-KRHHL-PVIAVFATHSHDDRAGDLSFYNQK-GIKTYATAKTNELLKKDG----------------KATSTEIIK  138
IND-3       MDTIQ-KRHNL-PVIAVFATHSHDDRAGDLSFFNNK-GIKTYATSKTNEFLKKDG----------------KATSTEIIK  138
IND-4       MDTIK-KRHNL-PVIAVFATHSHSDRAGDLSFYNKK-GIPTYATAKTNELLKKEG----------------KATSSKLTK  139
IND-5       MDTIK-KRHNL-PVIAVFATHSHDDRAGDLSFFNNK-GIKTYATSKTNEFLKKDG----------------KATSTEIIK  138
IND-6       MDTIK-KRHNL-PVVAVFATHSHDDRAGDLSFFNNK-GIKTYATPKTNQFLKRDG----------------KATSTELIK  138
IND-7       MDTIK-KRHNL-PVVAVFATHSHDDRAGDLSFFNNK-GIKTYATAKTNEFLKKDG----------------KATSTEIIK  138
                          :                            :

BBL No.       180       190       200       210       220       230       240       250
               |         |         |         |         |         |         |         |
IND-1       TGKPYRIGGEEFVVDFLGEGHTADNVVVWF---PKY---NVLDGGCLVKSNSATDLGYIKEANVEQWPKTINKLKAKYSK  212
IND-2       TGKPYKIGGEEFMVDFLGEGHTVDNVVVWF---PKY---KVLDGGCLVKSRTATDLGYTGEANVKQWPETMRKLKTKYAQ  212
IND-2a      TGKPYKIGGEEFMVDFLGEGHTVDNVVVWF---PKY---KVLDGGCLVKSRTATDLGYTGEANVKQWPETMRKLKTKYAQ  212
IND-3       TGKPYRIGGEEFVVDFLGEGHTADNVVVWF---PKY---NVLDGGCLVKSKAATDLGYIKEANVEQWPKTINKLKSKYSK  212
IND-4       IGKKYKIGGEEFTVDFLGEGHTADNVVVWF---PKY---NVLDGGCLVKSSAAVDLGYTGEANVEQWPATMKKLQAKYPS  213
IND-5       TGKPYRIGGEEFTVDFLGEGHTADNVVVWF---PKY---NVLDGGCLVKSNSATDLGYIKEANVEQWPITIDKLKAKYSK  212
IND-6       PQKPYRFGGEEFVVDFLGEGHTADNVVVWF---PKY---KVLDGGCLVKSNSATDLGYIKEANLEQWPKTMHKLKTKYSE  212
IND-7       TGKPYRIGGEEFVVDFLGEGHTADNVVVWF---PKY---NVLDGGCLVKSNSATDLGYIKEANVEQWPKTINKLKAKYSK  212
                        :                                                       :  :

BBL No.       260       270       280       290
               |         |         |         |
IND-1       ATLIIPGHDE-----------WKGGGHVEHTLE-LLNKK         239
IND-2       ATLVIPGHDE-----------WKGGGHVQHTLD-LLDKNKKPE     243
IND-2a      ATLVIPGHEE-----------WKGGGHVQHTLD-LLDKNKKPE     243
IND-3       ASLVIPGHDE-----------WKGGGHVKHTLE-LLNKK         239
IND-4       TAKVIPGHDE-----------WKGNDHVKHTLE-LLDQQKQ       242
IND-5       ATLIIPGHDD-----------WKGGGHVEHTLE-LLNKK         239
IND-6       AVLIIPGHDE-----------WKGGGHVEHTLE-LLDKK         239
IND-7       ATLIIPGHDE-----------WKGGGHVEHTLE-LLNKK         239
```

%identity

	IND-1	IND-2	IND-2a	IND-3	IND-4	IND-5	IND-6	IND-7
IND-1		80	79	91	72	92	87	99
IND-2			99	81	73	81	79	80
IND-2a				81	72	80	78	79
IND-3					72	92	70	72
IND-4						72	70	72
IND-5							89	92
IND-6								87
IND-7								

Fig. 1 Alignment of the amino acid sequence of IND-7 from *C. indologenes* with those of seven IND variants from *C. indologenes*. The IND variants are as follows: IND-1 (GenBank accession number: AF099139), IND-2 (AF219129), IND-2a (AF219130), IND-3 (AF219133), IND-4 (AF219135), IND-5 (AY504627) and IND-6 (AM087455). Sequence comparison was performed by aligning the protein amino acid sequences by use of the MULTALIN program (*66*). The class B metallo-β-lactamase numbering scheme is indicated above the sequences (*4*). Dashes indicate gaps introduced to optimize the alignment. Numbers on the right indicate numbers of amino acid residues from the N-terminus for each mature protein. Zinc(II)-coordinating residues are shaded in grey. Substitutions between IND-1 and IND-7 are circled. Substitutions between IND-5 and IND-7 are indicated by colons. The regions of loop 1 and loop 2 in IND-7 are underlined and double-underlined, respectively. The matrix at the bottom of the figure summarizes the levels of amino acid sequence identity.

Table I. Data collection and refinement statistics for IND-7.

Data collection	
Resolution (Å)	50.0–1.65 (1.71–1.65)
Wavelength (Å)	1.00
Unit-cell parameters (Å, °)	$a=77.6$, $b=74.3$, $c=47.4$, $\beta=99.4$
Space group	$C2$
Redundancy	3.7 (3.5)
Completeness (%)	99.9 (99.7)
R_{merge}[a]	4.3 (0.104)
No. of unique reflections	31,928 (901)
$I/\sigma(I)>$	48.5 (16.7)
Refinement statistics	
σcut-off	None
Resolution (Å)	38.3–1.65 (1.69–1.65)
No. of reflections used	30,314
B factors (Å^2)	
Average	13.5
Protein	11.0
Water	26.0
No. of non-H atoms[b]	
Protein	1,811
Water	327
R.m.s. deviation for ideal[c]	
Bond lengths (Å)	0.008
Angles (°)	1.09
$R_{working}$[d]	0.177 (0.221)
R_{free}[e]	0.200 (0.250)

[a]$R_{merge}=\sum_{hkl}\sum_i|I_i(hkl)-<I(hkl)>|/\sum_{hkl}\sum_i I_i(hkl)$, where $I_i(hkl)$ is the observed intensity for reflection for hkl and $<I(hkl)>$ is the average intensity calculated for reflection hkl from replicate data. [b]Per asymmetric unit. [c]RMSD.: root mean square differences. [d]$R_{working}=\sum_{hkl}||F_o|-|F_c||/\sum_{hkl}|F_o|$, where F_o and F_c are the observed and calculated structure factors, respectively. [e]$R_{free}=\sum_{hkl}||F_o|-|F_c||/\sum_{hkl}|F_o|$ for 5% of the data not used at any stage of structural refinement. Values in parentheses are for the last resolution shell.

bond distances and angles were 0.008 Å and 1.09°, respectively. A Ramachandran plot showed that 97.6% and 5.8% of the residues were in the most-favoured regions and in the additionally allowed regions, respectively, and 0.5% and 1.1% of those were in the generously allowed regions and in the disallowed regions, respectively. The exceptions were Asp50(33) and Asp84(66), which adopted ϕ and ψ angles of 79° and −51°, and 70° and 160°, respectively. Asp84 was buried in the protein and exhibited a strained main chain conformation, which is a commonly observed feature in the crystal structures of BcII, CcrA and IMP-1 metallo-β-lactamases (*28*, *32*, *35*). Therefore, it is thought that conservation of the conformation of Asp84 is important to the folding of metallo-β-lactamases.

The overall structure of IND-7 was found to be composed of five α-helixes and twelve β-strands, which fold into a four-layered αβ/βα sandwich structure (Fig. 2A). The dinuclear zinc(II) active site was located at the bottom of a shallow groove and was made up of the two zinc(II) ions (Zn1 and Zn2), the zinc(II) ion binding residues and two loops (loop 1 and loop 2). Loop 1, which is a typical feature of subclass B1 metallo-β-lactamases, was formed by residues at positions 60–66 (*51*) (BBL numbering, Figs 1 and 2A) between β2 and β3. This flexible loop is thought to be responsible for the tight binding of substrates and inhibitors in the dinuclear zinc(II) active site (*35*, *51–55*). In the IND-7 structure, loop 1 was well defined. Loop 2 was comprised residues at positions 221–241 (BBL numbering), positioned approximately opposite loop 1 cantered at about the zinc(II) binding site (Figs 1 and 2A). Thus, the overall structure of IND-7 was found to be similar to the previously solved structures of subclass B1 metallo-β-lactamases (*7*, *10*, *28–38*).

Coordination mode and occupancy of zinc(II) ions in the dinuclear zinc(II) active site

To understand the structural features of IND-7 in detail, the structures of IND-7 and structurally well-characterized CcrA from *B. fragilis*, which have 28% sequence homology (PDB code: 1ZNB; 1.85 Å resolution), were compared. As shown in Fig. 2B, superimposing the Cα atoms of IND-7 and molecule A in CcrA demonstrated a similarity in the protein folds with an overall RMSD of 1.7 Å, as mentioned above. Despite the similarity in the overall structures between these two enzymes, noticeable structural differences were found in the dinuclear zinc(II) active sites.

In the CcrA structure (Fig. 3A), Zn1 was coordinated with His116(99), His118(101), His196(162) and a water molecule or hydroxide ion (Wat1), forming a tetrahedral geometry, whereas Zn2 was coordinated with Asp120(103), Cys221(181), His263(223), one water molecule (Wat3, termed 'apical water') and Wat1, forming a trigonal bipyramidal geometry. The zinc(II) coordination geometry found in CcrA is mostly conserved in subclass B1 metallo-β-lactamases.

On the other hand, the zinc(II) coordination mode of IND-7 was different from the common feature. In the process of refinement of the IND-7 structure, we initially set the occupancies of Zn1 and Zn2 as 1.0 and refined their B-factors. As the B-factor of Zn2 (15.6 Å^2) was relatively higher than that of Zn1 (9.3 Å^2), occupancies for Zn1 and Zn2 were reset as 1.0 and 0.7, respectively, for subsequent refinement. The final B-factors equalled ~9.3 Å^2 for Zn1 and 12.3 Å^2 for Zn2. The average B-factor of the residues involved in the zinc(II) coordination, His116(96), His118(98), Asp120(100), His196(159), Cys221(178) and His263(220), was 7.1 Å^2. These results suggested that the affinity of Zn2 was lower than that of Zn1, and that Zn2 tended to escape from the dinuclear zinc(II) active site of IND-7 Moreover, a $2|F_o|-|F_c|$ electron density map around the Zn2 site (Fig. 3B) clearly showed the existence of both conformations in the side chains of Cys221(178) and His263(220), where the occupancies of Cys221A(178) and His263A(220) were refined by 0.7, and those of Cys221B(178) and His263B(220) were refined by 0.3. The former was a Zn2-coordinated form, whereas the latter was a Zn2-uncoordinated form. Interestingly, in the side chain of Asp120(100), a zinc(II) ligand, no disorder was observed, which was fixed through the interactions of Zn2 and Wat1 (*vide infra*). This finding indicates that Asp120 played an important role in helping to orient a zinc(II)-bound hydroxide ion for a nucleophilic attack on the CO group of the β-lactam ring.

The coordination geometry around Zn1 (Fig. 3B) was a distorted trigonal bipyramid with $\tau=0.88$

Table II. Zinc(II)-ligand distances (Å) and angles (°) for IND-7 and CcrA metallo-β-lactamases.

		IND-7	CcrA[a]	
Zn(II)-ligand[b]		Distances		
Zn1	His116NE2	2.1	2.1/2.2	
	His118ND1	2.0	2.0/2.1	
	His196NE2	2.0	2.0/2.0	
	O(Wat1)	1.9	1.9/2.0	
	O(Wat2)	2.6		
Zn2	Asp120OD2	2.1	2.3/2.1	
	Cys221ASG	2.2	2.3/2.4	
	His263ANE2	2.1	2.1/2.2	
	O(Wat1)	2.1	2.1/2.2	
	O(Wat3)		2.3/2.2	
Zn1	Zn2	3.6	3.5/3.5	
Ligand-Zn(II)-Ligand[b]			Angles	
His116(96)NE2	Zn1	His118ND1	99	105/100
	Zn1	His196NE2	102	100/106
	Zn1	O(Wat1)	108	119/111
His118(98)ND1	Zn1	His196NE2	116	107/108
	Zn1	O(Wat1)	116	112/109
His196(159)NE2	Zn1	O(Wat1)	113	113/121
O(Wat2)	Zn1	His116NE2	169	
	Zn1	His118ND1	71	
	Zn1	His196NE2	88	
	Zn1	O(Wat1)	73	
Asp120(100)OD2	Zn2	Cys221ASG	113	97/97
	Zn2	His263ANE2	91	86/82
	Zn2	O(Wat1)	94	86/81
Cys221A(179)SG	Zn2	His263ANE2	110	107/110
	Zn2	O(Wat1)	118	115/117
His263A(220)NE2	Zn2	O(Wat1)	125	138/132
O(Wat3)	Zn2	Asp120OD2		161/164
	Zn2	Cys221ASG		101/110
	Zn2	His263ANE2		83/89
	Zn2	O(Wat1)		92/95

[a]The distances and angles for CcrA metallo-β-lactamase are quoted for molecules A and B in the asymmetric unit. [b]Ligand numbers are indicated by the BBL numbering scheme and numbers of amino acid resides from the N-terminus for each mature protein are omitted for simplification.

[structural parameter $\tau = (\beta - \alpha)/60$) (*56*)], where $\alpha = 116°$ for His118(98)ND1–Zn1 – His196(159)NE2 and $\beta = 169°$ for O(Wat2) – Zn1 – His116(96)NE2 were the two basal angles ($\beta \geq \alpha$) representing the change in trigonal distortion from a square pyramidal geometry: $\tau = 0$ for an ideal square pyramid and 1 for an ideal trigonal bipyramid. Two His residues, His118(98) and His196(159), and either one oxygen from a water molecule or a hydroxide ion (labeled Wat1) made a trigonal plane (the average angle of the corresponding angles was 115°). Wat1, which is thought to act as the attacking nucleophile on the CO group of the β-lactam ring (*32*, *57*, *58*), bridged to both Zn1 and Zn2, and also formed a hydrogen bond with one oxygen atom of Asp120(100) with a distance of 2.7 Å. The apical positions were occupied by His116(96) and Wat2, where Wat2 weakly interacted with Zn1 at a distance of 2.6 Å [the average Zn – Wat bond distance in zinc(II) enzymes is reportedly 2.2 Å (*59*)]. In the crystal structure of VIM-2 metallo-β-lactamase, Zn1 is also coordinated to five ligands in a distorted trigonal bipyramidal geometry (*37*), as seen in the IND-7 structure. However, the Zn1 – Wat bond distance (2.8 Å) at the apical position was longer by 0.2 Å than that of IND-7 (Zn1 – Wat2). These observations suggest that Wat2 can more easily accommodate replacement by the Zn1 coordination sphere upon uptake of substrates and inhibitors. We expected the coordination structure of the dinuclear zinc(II) active site in IND-7, especially pentacoordination at the Zn1 site, to be of major benefit to a favourable Michaelis complex, because Wat2 was thought to be the carbonyl oxygen atom of the β-lactam ring that interacted with Zn1 upon formation of the Michaelis complex (Fig. 4).

The Zn1–His and Zn1–Wat1 bond distances were 2.0 – 2.1 Å and 1.9 Å, respectively, which were almost identical to those found in CcrA (2.0 – 2.2 Å for Zn1 – His and 1.9 – 2.0 Å for Zn1 – O, respectively). Zn2 was tetrahedrally coordinated with Asp120(100), Cys221A(178), His263A(220), and Wat1, with bond distances of 2.1 Å (Fig. 3B), and 'the apical water Wat3', observed in CcrA, was missing from the IND-7 structure. The Zn2 – Wat1 bond distance of 2.1 Å was somewhat longer than that of Zn1–Wat1 and this tendency was also found in CcrA. The ligand–Zn2–ligand bond angles of 91–125° (the average angle; 109°) were close to the optimal tetrahedral angles. The Zn1 – Zn2 distance was 3.6 Å and this bond distance was close to that of CcrA (3.5 Å). Thus, the zinc(II) coordination geometry was notably

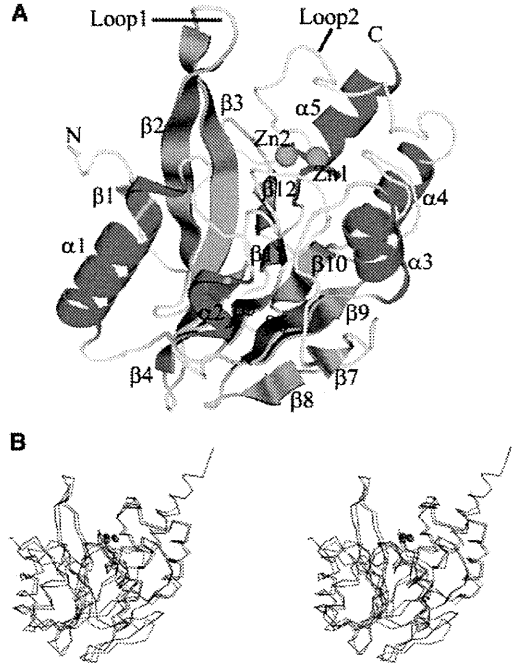

Fig. 2 Overall structure of IND-7 from *C. indologenes*. (A) A ribbon diagram of IND-7 is shown with the secondary structures labeled. α-Helices, β-strands and the loops are shown in red, green and yellow, respectively. Zinc(II) ions are represented as orange spheres. The figure was prepared with MolFeat software (FiatLux Corporation). (B) Superposition of the C_α tracing of IND-7 (red) with CcrA from *B. fragilis* [blue, PDB code: 1ZNB, (*32*)]. In the CcrA structure, only molecule A is depicted.

different from those of other crystal structures of subclass B1 metallo-β-lactamases, which includes CcrA.

Role of Arg121 and hydrogen-bonding networks around the dinuclear zinc(II) active site

Arg121 is well conserved in IND variants (*39*, *40*), VIM variants (*20*), BlaB (*60*) and BcII (*7*, *32*), and is thought to be responsible for the reduced binding affinity for Zn2 (*29*, *33*, *35*). Indeed, BcII metallo-β-lactamase has a binding affinity that differs from that of the two zinc(II) binding sites (*61–63*). By contrast, residues at position 121 in CcrA and IMP variants are occupied by Cys121(104) and Ser121(82), respectively, and these metallo-β-lactamases display high binding affinity at both the Zn1 and Zn2 sites (*64*, *65*).

As seen in Fig. 3C, a positively charged guanidinyl group of Arg121(101) was situated below the floor of the Zn2 site. A $2|F_o| - |F_c|$ electron density map clearly indicated Arg121(101) alternated in the crystal, and the conformations Arg121A(101) and Arg121B(101) fit the map well. The former corresponded to a Zn2-coordinated form of Cys221(178) and His263(220), whereas the latter corresponded to a Zn2-uncoordinated form with no bound Zn2. Therefore, the corresponding atoms in the two conformations were refined with occupancies of 0.7 and 0.3, respectively. In Arg121A(101), the electrostatic repulsion between a positively charged bulky guanidinyl group of Arg121 and Zn2 cause movement of the guanidinyl group to move away from Zn2 [4.7 Å from Arg121A(101)NE and 5.7 Å from Arg121A(101)NH2], where the guanidinyl group is maintained by four hydrogen bonds between Asn70(52), Ser71(*53*), Asp84(66) and Asp120(100): Arg121A(101)NE Asp120(100)O = 2.8 Å, Arg121A (101)NH1 · Asp84(66)OD2 = 3.2 Å, Arg121A(101) NH2 · Asn70(52) = 2.7 Å and Arg121A(101)NH2 · Ser71(*53*)OG = 3.0 Å. Ser71(53) is conserved in IND-1, IND-3, and IND-5–IND-7 but is Gly in IND-2, IND-2a, and IND-4 (Fig. 1). The substitution of residues at position 71(*53*) in IND variants is expected to have an effect on the changing of the binding affinity of Zn2 and on the hydrolysis of β-lactams.

In Arg121B(101), with a rotation of the CG–CD bond of the side chain in Arg121B(101), the plane formed by the atoms CD, NE, NH1 and NH2 of Arg121B(101) was nearly perpendicular to the corresponding plane of Arg121A(101) and the guanidinyl group of Arg121B(101) lay close to the dinuclear zinc(II) active site [3.5 Å from Arg121B(101)NE and 3.6 Å from Arg121B(101)NH2]. The guanidinyl group made four hydrogen bonds with Asn70(*52*), Asp84(66), Asp120(100) and Gly262(219): Arg121B (101)NE Asp120(100)OD2 = 2.9 Å, Arg121B(101) NH1 Asn70(52)O = 3.0 Å, Arg121B(101)NH1 Asp84 (66)OD2 = 3.2 Å and Arg121B(101)NH2 Gly262 (219)O = 2.7 Å, of which two hydrogen bonds of Arg121B(101) with Asp120(100) and Gly262(219) pulled the guanidinyl group close to the dinuclear zinc(II) active site. These observations highlight the importance of Arg121(101) for the binding affinity of Zn2 by cooperation between the electrostatic effect and the change in the hydrogen-bonding network. In addition, Arg121(101) also appeared to partially contribute to the preservation of the moderate orientation of Asp120(100) relative to Zn2.

We compared the hydrogen-bonding networks around the dinuclear zinc(II) active site to estimate the primary cause of the differences in coordination structure between IND-7 and CcrA metallo-β-lactamases.

In CcrA, the side chain NZ of Lys224(184) produced hydrogen-bonding networks with Wat3 coordinated to Zn2, the side chain ND1 of His196(162), and the main chain oxygen atoms of Cys221(181), Ile231(191) and Asn233(193) through well-ordered water molecules (Fig. 5A). Lys224 located on loop 2 was assumed to interact with the carboxylate of the β-lactams (*32*, *35*). Moreover, the side chain of ND2 of Asn233(193) formed a hydrogen-bonding network with bridging water between Zn1 and Zn2, Wat1, via a water molecule. Conversely, the hydrogen-bonding networks in IND-7 were somewhat different from those of CcrA (Fig. 5B). Lys224(181), which was ~7 Å away from the zinc(II) active site, did not participate in the hydrogen-bonding networks between the bulk water molecules. In the case of IND-7, Asn233(193) in CcrA was replaced with Tyr233(190), which was located on loop 2. Tyr233(190) rotated ~74° around the CB–CG bond and the hydroxy group of the phenyl ring was ~8 Å away from Zn1. The main chain oxygen atoms of Leu231(188) and Tyr233(190) were hydrogen bonded to a water molecule, which is

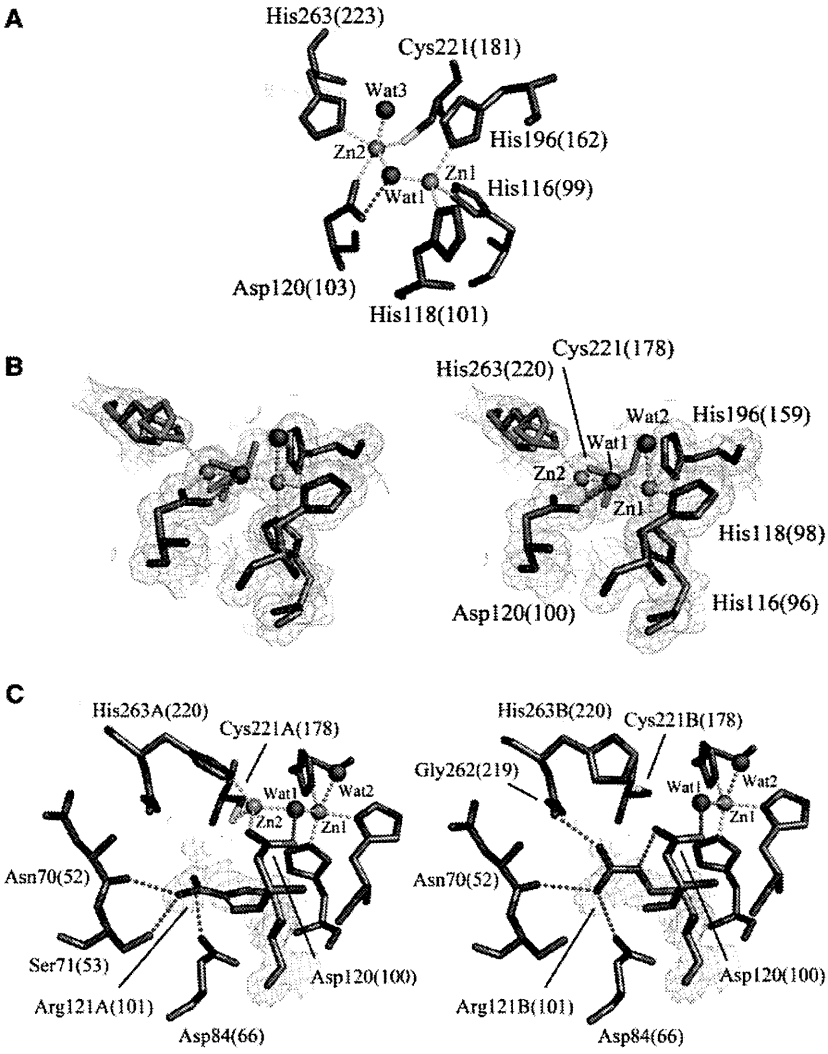

Fig. 3 Comparison of the dinuclear zinc(II) active site structures in CcrA from *B. fragilis* [PDB code: 1ZNB, (32)] and IND-7 from *C. indologenes*. (A) Active site structure in CcrA; only molecule A is depicted. Zn1 is tetrahedrally coordinated with His116(99), His118(101), His196(162) and Wat1. Zn2 is trigonal-bipyramidally coordinated with Asp120(103), Cys221(181), His263(223), Wat1 and Wat2. Zinc(II) ions and water molecules are presented as orange and red spheres, respectively. Carbon, oxygen, nitrogen and sulphur atoms are shown in grey, red, blue and yellow, respectively. Zn(II) – ligand bonds are shown as yellow dotted lines. The hydrogen bond is shown as a red dotted line. (B) Stereo view of the active site in IND-7. The electron density map (green mesh) is shown contoured at the 1.0σ level in the $2|F_o|-|F_c|$ map. Zinc(II) ions and water molecules are shown as orange and red spheres, respectively. Carbon, oxygen, nitrogen and sulphur atoms are shown in grey, red, blue and yellow, respectively. Zn(II)–ligand bonds, with the exception of the Zn(II)–Wat2 bond, are shown as yellow dotted lines. The Zn(II)–Wat2 bond is shown as a green dotted line. The hydrogen bond is shown as a red dotted line. The occupancies of Zn1 and Zn2 are refined with 1.0 and 0.7, respectively. Cys221(178) and His263(220) adopted alternative conformations in the IND-7 structure [Cys221A(178) and His263A(220), and Cys221B(178) and His263B(220)]. The occupancies of Cys221A(178) and His263A(220) (magenta sticks) are refined with 0.7 in each case, whereas those of Cys221B(178) and His263B(220) (orange sticks) are refined with 0.3 in each. Zn1 is trigonal-bipyramidally coordinated with His116(96), His118(98), His196(159), Wat1 and Wat2. Zn2 is tetrahedrally coordinated with Asp120(100), Cys221A(178), His263A(220) and Wat1. Unlike the CcrA structure, 'the apical water' Wat3 is absent from the Zn2 site. (C) Alternative conformations of Arg121(101), Arg121A(101) and Arg121B(101). The electron density map (green mesh) of Arg121(101) is shown contoured at the 1.0σ level in $2|F_o|-|F_c|$ map. Of the two conformations, Arg121A(101) is shown to the left, whereas Arg121B(101) is shown to the right. The former was a Zn2-coordinated form of Cys221(178) and His263(220), whereas the latter was a Zn2-uncoordinated form with no bound Zn2. The occupancies of Arg121A(101) and Arg121B(101) are refined with 0.7 and 0.3, respectively. Carbon, oxygen, nitrogen and sulphur atoms are shown in grey, red, blue and yellow, respectively. Zn(II)–ligand bonds, with the exception of Zn(II)–Wat2, are shown as yellow dotted lines. The Zn(II)–Wat2 bond is shown as a green dotted line. Hydrogen bonds are shown as red dotted lines. The figures were prepared with *PyMol* software (http://pymol.sourceforgen.net/).

occupied in a position equivalent to that of a water molecule in the CcrA structure, forming hydrogen-bonding networks with Wat1 and Wat2 that was coordinated to Zn1, the side chain ND1 of His196(159), and the main chain oxygen atoms of Cys221(181). Interestingly, Wat2 formed two hydrogen bonds with two water molecules, one of which interacted with Wat1 to achieve formation of a hydrogen-bonding network between Wat1 and Wat2—the other was linked to bulk water molecules. This seemed to be one of the factors affecting the structural change in the Zn1 coordination sphere, which was also thought to be closely related to the difference in enzymatic activity.

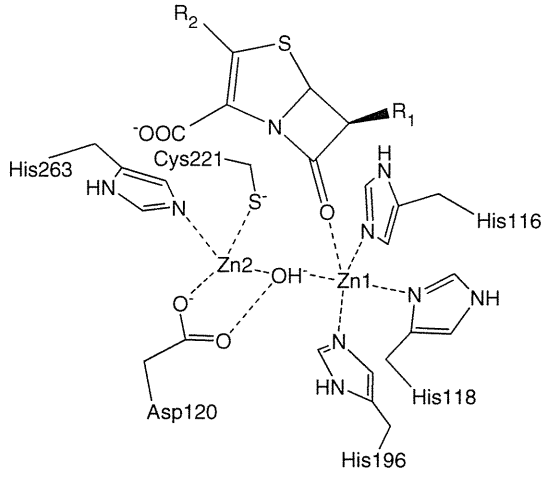

Fig. 4 A model of the Michaelis complex for β-lactam bound to subclass B1 metallo-β-lactamase.

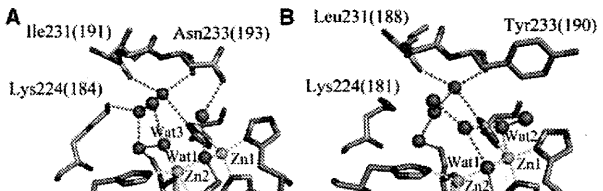

Fig. 5 Comparison of hydrogen-bonding networks between (A) CcrA from *B. fragilis* [PDB code: 1ZNB, (32)] and (B) IND-7 *C. indologenes* in the vicinity of the dinuclear zinc(II) active sites. Carbon, oxygen, nitrogen and sulphur atoms are shown in grey, red, blue and yellow, respectively. Zn(II)–ligand bonds, with the exception of Zn(II)–Wat2, are shown as yellow dotted lines. The Zn(II)–Wat2 bond is shown as a green dotted line. Hydrogen bonds are shown as red dotted lines. The figures were prepared with *PyMol* software (http://pymol.sourceforgen.net/).

Structure-activity relationship between IND-2 and IND-5 deduced from the IND-7 structure

In 2007, Perilli *et al.* (*40*) isolated IND-5 from a clinical isolate of *C. indologenes* and conducted kinetic studies on the hydrolysis of various β-lactams against IND-5 metallo-β-lactamase. From a comparison of kinetic parameters of IND-5 with those of IND-2, they reported that the catalytic efficiencies (k_{cat}/K_m) of IND-2 for imipenem and meropenem were ~25- and 13-fold higher than those of IND-5, respectively. On the basis of the comparison of the amino acid sequence of IND-5 with those of IND variants, including IND-2, Perilli *et al.* assumed that the residue at position 265 (BBL numbering) might be involved in the drastic reduction in catalytic efficiency of IND-5, compared with that of IND-2 (*39*, *40*): Glu265(222) was well conserved in all IND variants with the exception of IND-5 [in this case, Asp265(222)] and was located close to His263(220), which is a Zn2 ligand.

As shown in Fig. 1, IND-7 shared 92% amino acid identity with the IND-5 of sixteen amino acid substitutions: Ser21(4)Lys, Lys23(6)Tyr, Ile26(9)Met, Ile29(12)Met, Leu30(13)Met, Ser32(15)Ala, Phe34(17)Met, Ala35(*18*)Phe and Ser36(19)Asn in the signal peptide region; and, Met72(54)Val, Val90(72)Ala, Val110(90)Ile, Ala140(119)Ser, Val188(151)Thr, Lys244(201)Ile, Asn247(204)Asp and Glu265(222)Asp. Extrapolating from the determined IND-7 structure, most of the amino acid substitutions of IND-5 were expected to be located either on the surface of the protein or far from the active site. Of these residues, Glu265(222) was located ~8 Å from the dinuclear zinc(II) active site. The backbone CO of Glu265(222) were hydrogen-bonded to the side chain OG of Ser225(182) at distances of 2.6 Å, but the side chain of Glu265(222) was turned to face the surface of the protein. Therefore, the side chain was not likely to influence the catalytic efficiency of IND-5 by Glu-to-Asp substitution at position 265. One possibility affecting the enzymatic activity of the mutant might have been the residue at position 235 (BBL numbering), which was located almost on top of loop 2 at a distance of ~9 Å from Zn1 and Zn2. In IND-1, IND-5 and IND-7, the residue at position 235 was Lys, whereas, for IND-2 the residue at the same position was Gly. Lys235(192) in the IND-7 structure had a strained main chain conformation, with ϕ and ψ angles of −60° and −29°, respectively. However, the Lys-to-Gly substitution at position 235 in IND-2 may have increased the degree of rotation about the ϕ and ψ angles, compared with IND-5, and caused the movement of loop 2 to access the conserved residue in all IND variants, Tyr233(190), of the hydrophobic pocket. Thus, the mutation at position 235 appeared to trigger changes in the mobility of the loop and in the uptake of the substrate to the active site, leading to a difference in the enzymatic activity.

In conclusion, we determined the crystal structure of IND-7 metallo-β-lactamase of *C. indologenes*. As a consequence, the precise coordination mode around the dinuclear zinc(II) active site was ascertained, and its coordination mode appeared to be quite different from those of the well-characterized metallo-β-lactamases, as determined by X-ray crystallography. It was predicted that the hydrogen-bonding interaction between Arg121(101) and Gly262(219) would influence conformational flexibility of His263(220) and, as the result, the fixation of His263(220) to Zn2 by this interaction did contribute to the binding affinity of Zn2 and to the enzymatic performance. Finally, the residue at position 235 of loop 2, rather than Glu-to-Asp substitution at position 265, might be critical to altering the enzymatic activity in the IND variants.

Funding

Aspects of the present study related to cloning, overexpression, purification, crystal optimization and X-ray diffraction analysis of the enzyme were supported by Grants from the Ministry of Health, Labor, and Welfare of Japan (H18-Shinkou-11 and H21-Shinkou-Ippan-008). A preliminary X-ray crystallographic analysis was supported by a Grant from the Ohyama Health Foundation, Inc. (to Y. Yamaguchi).

Conflict of interest

None declared.

References

1. Fisher, J.F., Meroueh, S.O., and Mobashery, S. (2005) Bacterial resistance to β-lactam antibiotics: Compelling opportunism, compelling opportunity. *Chem. Rev.* **105**, 395–424
2. Frère, J.-M. (1995) Beta-lactamases and bacterial resistance to antibiotics. *Mol. Microbiol.* **16**, 385–395
3. Wilke, M.S., Lovering, A.L., and Strynadka, N.C. (2005) Beta-lactam antibiotic resistance: a current structural perspective. *Curr. Opin. Microbiol.* **8**, 525–533
4. Galleni, M., Lamotte-Brasseur, J., Rossolini, G.M., Spencer, J., Dideberg, O., and Frère, J.-M. The metallo-β-lactamase working group. (2001) Standard numbering scheme for class B β-lactamases. *Antimicrob. Agents Chemother.* **45**, 660–663
5. Garau, G., Di Guilmi, A.M., and Hall, B.G. (2005) Structure-based phylogeny of the metallo-β-lactamases. *Antimicrob. Agents Chemother.* **49**, 2778–2784
6. Rasmussen, B.A. and Bush, K. (1997) Carbapenem-hydrolyzing β-lactamases. *Antimicrob. Agents Chemother.* **41**, 223–232
7. Fabiane, S.M., Sohi, M.K., Wan, T., Payne, D.J., Bateson, J.H., Mitchell, T., and Sutton, B.J. (1998) Crystal structure of the zinc-dependent β-lactamase from *Bacillus cereus* at 1.9 Å resolution: binuclear active site with features of a mononuclear enzyme. *Biochemistry* **37**, 12404–12411
8. Toney, J.H., Hammond, G.G., Fitzgerald, P.M.D., Sharma, N., Balkovec, J.M., Rouen, G.P., Olson, S.H., Hammond, M.L., Greenlee, M.L., and Gao, Y.-D. (2001) Succinic acids as potent inhibitors of plasmid-borne IMP-1 metallo-β-lactamase. *J. Biol. Chem.* **276**, 31913–31918
9. García-Sáez, I., Mercuri, P.S., Papamicael, C., Kahn, R., Frère, J.-M., Galleni, M., Rossolini, G.M., and Dideberg, O. (2003) Three-dimensional structure of FEZ-1, a monomeric subclass B3 metallo-β-lactamase from *Fluoribacter gormanii,* in native form and in complex with D-captopril. *J. Mol. Biol.* **325**, 651–660
10. Murphy, T.A., Catto, L.E., Halford, S.E., Hadfield, A.T., Minor, W., Walsh, T.R., and Spencer, J. (2006) Crystal structure of *Pseudomonas aeruginosa* SPM-1 provides insights into variable zinc affinity of metallo-β-lactamases. *J. Mol. Biol.* **357**, 890–903
11. Felici, A., Amicosante, G., Oratore, A., Strom, R., Ledent, P., Joris, B., Fanuel, L., and Frère, J.-M. (1993) An overview of the kinetic parameters of class B β-lactamases. *Biochem. J.* **291**, 151–155
12. Garau, G., Bebrone, C., Anne, C., Galleni, M., Frère, J.M., and Dideberg, O. (2005) A metallo-β-lactamase enzyme in action: crystal structures of the monozinc carbapenemase CphA and its complex with biapenem. *J. Mol. Biol.* **345**, 785–795
13. Sharma, N.P., Hajdin, C., Chandrasekar, S., Bennett, B., Yang, K.W., and Crowder, M.W. (2006) Mechanistic studies on the mononuclear Zn(II)-containing metallo-β-lactamase ImiS from *Aeromonas sobria. Biochemistry* **45**, 10729–10738
14. Crawford, P.A., Yang, K.W., Sharma, N., Bennett, B., and Crowder, M.W. (2005) Spectroscopic studies on cobalt(II)-substituted metallo-β-lactamase ImiS from *Aeromonas veronii* bv. *sobria. Biochemistry* **44**, 5168–5176
15. Bebrone, C., Anne, C., De Vriendt, K., Devreese, B., Rossolini, G.M., Van Beeumen, J., Frere, J.M., and Galleni, M. (2005) Dramatic broadening of the substrate profile of the *Aeromonas hydrophila* CphA metallo-β-lactamase by site-directed mutagenesis. *J. Biol. Chem.* **280**, 28195–28202
16. Walsh, T.R., Gamblin, S., Emery, D.C., MacGowan, A.P., and Bennett, P.M. (1996) Enzyme kinetics and biochemical analysis of ImiS, the metallo-β-lactamase from *Aeromonas sobria* 163a. *J. Antimicrob. Chemother.* **37**, 423–431
17. Segatore, B., Massidda, O., Satta, G., Setacci, D., and Amicosante, G. (1993) High specificity of *cphA*-encoded metallo-β-lactamase from *Aeromonas hydrophila* AE036 for carbapenems and its contribution to β-lactam resistance. *Antimicrob. Agents Chemother.* **37**, 1324–1328
18. Walsh, T.R., Toleman, M.A., Poirel, L., and Nordmann, P. (2005) Metallo-β-lactamases: the quiet before the storm? *Clin. Microbiol. Rev.* **18**, 306–325
19. Senda, K., Arakawa, Y., Ichiyama, S., Nakashima, K., Ito, H., Ohsuka, S., Shimokata, K., Kato, N., and Ohta, M. (1996) PCR detection of metallo–βlactamase gene (blaIMP) in gram-negative rods resistant to broad-spectrum β-lactams. *J. Clin. Microbiol.* **34**, 2909–2913
20. Lauretti, L., Riccio, M.L., Mazzariol, A., Cornaglia, G., Amicosante, G., Fontana, R., and Rossolini, G.M. (1999) Cloning and characterization of bla_{VIM}, a new integron-borne metallo-β-lactamase gene from a *Pseudomonas aeruginosa* clinical isolate. *Antimicrob. Agents Chemother.* **43**, 1584–1590
21. Lim, H.M., Pene, J.J., and Shaw, R.W. (1988) Cloning, nucleotide sequence, and expression of the *Bacillus cereus* 5/B/6 β-lactamase II structural gene. *J. Bacteriol.* **170**, 2873–2878
22. Rossolini, G.M., Franceschini, N., Lauretti, L., Caravelli, B., Riccio, M.L., Galleni, M., Frère, J.M., and Amicosante, G. (1999) Cloning of a *Chryseobacterium* (*Flavobacterium*) *meningosepticum* chromosomal gene ($blaA_{(CME)}$) encoding an extended-spectrum class A β-lactamase related to the *Bacteroides cephalosporinases* and the VEB-1 and PER β-lactamases. *Antimicrob. Agents Chemother.* **43**, 2193–2199
23. Wang, Z., Fast, W., and Benkovic, S.J. (1998) Direct observation of an enzyme-bound intermediate in the catalytic cycle of the metallo-β-lactamase from *Bacteroides fragilis. J. Am. Chem. Soc.* **120**, 10778–10789
24. Bellais, S., Léotard, S., Poirel, L., Naas, T., and Nordmann, P. (1999) Molecular characterization of a carbapenem-hydrolyzing β-lactamase from *Chryseobacterium* (*Flavobacterium*) *indologenes. FEMS Microbiol. Lett.* **171**, 127–132
25. Osano, E., Arakawa, Y., Wacharotayankun, R., Ohta, M., Horii, T., Ito, H., Yoshimura, F., and Kato, N. (1994) Molecular characterization of an enterobacterial metallo β-lactamase found in a clinical isolate of *Serratia marcescens* that shows imipenem resistance. *Antimicrob. Agents Chemother.* **38**, 71–78
26. Toleman, M.A., Simm, A.M., Murphy, T.A., Gales, A.C., Biedenbach, D.J., Jones, R.N., and Walsh, T.R. (2002) Molecular characterization of SPM-1, a novel metallo-β-lactamase isolated in Latin America: report from the SENTRY antimicrobial surveillance programme. *J. Antimicrob. Chemother.* **50**, 673–679
27. Castanheira, M., Toleman, M.A., Jones, R.N., Schmidt, F.J., and Walsh, T.R. (2004) Molecular characterization of a β-lactamase gene, bla_{GIM-1}, encoding a new subclass of metallo-β-lactamase. *Antimicrob. Agents Chemother.* **48**, 4654–4661
28. Carfi, A., Pares, S., Duée, E., Galleni, M., Duez, C., Frère, J.-M., and Dideberg, O. (1995) The 3-D structure

of a zinc metallo-β-lactamase from *Bacillus cereus* reveals a new type of protein fold. *EMIBO J.* **14**, 4914–4921
29. Carfi, A., Duee, E., Galleni, M., Frère, J.-M., and Dideberg, O. (1998) 1.85 Å resolution structure of the zinc (II) β-lactamase from *Bacillus cereus*. *Acta Cryst.* **D54**, 313–323
30. Chantalat, L., Duée, E., Galleni, M., Frère, J.M., and Dideberg, O. (2000) Structural effects of the active site mutation cysteine to serine in *Bacillus cereus* zinc-β-lactamase. *Protein Sci.* **9**, 1402–1406
31. García-Sáez, I., Hopkins, J., Papamicael, C., Franceschini, N., Amicosante, G., Rossolini, G.M., Galleni, M., Frère, J.-M., and Dideberg, O. (2003) The 1.5-Å structure of *Chryseobacterium meningosepticum* zinc β-lactamase in complex with the inhibitor, D-captopril *J. Biol. Chem.* **278**, 23868–23873
32. Concha, N.O., Rasmussen, B.A., Bush, K., and Herzberg, O. (1996) Crystal structure of the wide-spectrum binuclear zinc β-lactamase from *Bacteroides fragilis*. *Structure* **4**, 823–836
33. Carfi, A., Duée, E., Paul-Soto, R., Galleni, M., Frère, J.-M., and Dideberg, O. (1998) X-ray structure of the ZnII β-lactamase from *Bacteroides fragilis* in an orthorhombic crystal form. *Acta Cryst.* **D54**, 45–57
34. Fitzgerald, P.M.D., Wu, J.K., and Toney, J.H. (1998) Unanticipated inhibition of the metallo-β-lactamase from *Bacteroides fragilis* by 4-morpholineethanesulfonic acid (MES): A crystallographic study at 1.85-Å resolution. *Biochemistry* **37**, 6791–6800
35. Concha, N.O., Janson, C.A., Rowling, P., Pearson, S., Cheever, C.A., Clarke, B.P., Lewis, C., Galleni, M., Frère, J.-M., Payne, D.J., Bateson, J.H., and Abdel-Meguid, S.S. (2000) Crystal structure of the IMP-1 metallo β-lactamase from *Pseudomonas aeruginosa* and its complex with a mercaptocarboxylate inhibitor: binding determinants of a potent, broad-spectrum inhibitor. *Biochemistry* **39**, 4288–4298
36. Kurosaki, H., Yamaguchi, Y., Yasuzawa, H., Jin, W., Yamagata, Y., and Arakawa, Y. (2006) Probing, inhibition, and crystallographic characterization of metallo-β-lactamase (IMP-1) with fluorescent agents containing dansyl and thiol groups. *Chem. Med. Chem.* **1**, 969–972
37. Garcia-Saez, I., Docquier, J.D., Rossolini, G.M., and Dideberg, O. (2008) The three-dimensional structure of VIM-2, a Zn-β-lactamase from *Pseudomonas aeruginosa* in its reduced and oxidised form. *J. Mol. Biol.* **375**, 604–611
38. Yamaguchi, Y., Jin, W., Matsunaga, K., Ikemizu, S., Yamagata, Y., Wachino, J., Shibata, N., Arakawa, Y., and Kurosaki, H. (2007) Crystallographic investigation of the inhibition mode of a VIM-2 metallo-β-lactamase from *Pseudomonas aeruginosa* by a mercaptocarboxylate inhibitor. *J. Med. Chem.* **50**, 6647–6653
39. Bellais, S., Poirel, L., Leotard, S., Naas, T., and Nordmann, P. (2000) Genetic diversity of carbapenem-hydrolyzing metallo-β-lactamases from *Chryseobacterium* (*Flavobacterium*) *indologenes*. *Antimicrob. Agents Chemother.* **44**, 3028–3034
40. Perilli, M., Caporale, B., Celenza, G., Pellegrini, C., Docquier, J.D., Mezzatesta, M., Rossolini, G.M., Stefani, S., and Amicosante, G. (2007) Identification and characterization of a new metallo-β-lactamase, IND-5, from a clinical Isolate of *Chryseobacterium indologenes*. *Antimicrob. Agents Chemother.* **51**, 2988–2990
41. Zeba, B., De Luca, F., Dubus, A., Delmarcelle, M., Simporé, J., Nacoulma, O.G., Rossolini, G.M., Frère, J.-M., and Docquier, J.-D. (2009) IND-6, a highly divergent IND-type metallo-β-lactamase from *Chryseobacterium indologenes* strain 597 isolated in Burkina Faso. *Antimicrob. Agents Chemother.* **53**, 4320–4326
42. Hsueh, P.R., Teng, L.J., Ho, S.W., Hsieh, W.C., and Luh, K.T. (1996) Clinical and microbiological characteristics of *Flavobacterium indologenes* infections associated with indwelling devices. *J. Clin. Microbiol.* **34**, 1908–1913
43. Otwinowski, Z. and Minor, W. (1997) Processing of X-ray diffraction data collected in oscillation mode *Methods Enzymol. 276,* 307–326
44. Navaza, J. (1994) *AMoRe*: an automated package for molecular replacement. *Acta Cryst.* **A50**, 157–163
45. Vagin, A. and Teplyakov, A. (1997) *MOLREP*: an automated program for molecular replacement. *J. Appl. Cryst.* **30**, 1022–1025
46. Collaborative Computational Project Number 4. (1994) The CCP4 suite: Programs for protein crystallography. *Acta Cryst.* **D50**, 760–763
47. Jones, T.A., Zou, J.-Y., Cowan, S.W., and Kjeldgaard, M. (1991) Improved methods for building protein models in electron density maps and the location of errors in these models. *Acta Cryst.* **A47**, 110–119
48. Emsley, P. and Cowtan, K. (2004) *Coot*: model-building tools for molecular graphics. *Acta Cryst.* **D60**, 2126–2132
49. Brünger, A.T., Adams, P.D., Clore, G.M., DeLano, W.L., Gros, P., Grosse-Kunstleve, R.W., Jiang, J.-S., Kuszewski, J., Nilges, M., Pannu, N.S., Read, R.J., Rice, L.M., Simonson, T., and Warren, G.L. (1998) *Crystallography & NMR system*: a new software suite for macromolecular structure determination. *Acta Cryst.* **D54**, 905–921
50. Murshudov, G.N., Vagin, A.A., and Dodson, E.J. (1997) Refinement of macromolecular structures by the maximum-likelihood method. *Acta Cryst.* **D53**, 240–255
51. Moali, C., Anne, C., Lamotte-Brasseur, J., Groslambert, S., Devreese, B., Van Beeumen, J., Galleni, M., and Frère, J.-M. (2003) Analysis of the importance of the metallo-β-lactamase active site loop in substrate binding and catalysis. *Chem. Biol.* **10**, 319–329
52. Huntley, J.J.A., Scrofani, S.D.B., Osborne, M.J., Wright, P.E., and Dyson, H.J. (2000) Dynamics of the metallo-β-lactamase from *Bacteroides fragilis* in the presence and absence of a tight-binding inhibitor. *Biochemistry* **39**, 13356–13364
53. Huntley, J.J., Fast, W., Benkovic, S.J., Wright, P.E., and Dyson, H.J. (2003) Role of a solvent-exposed tryptophan in the recognition and binding of antibiotic substrates for a metallo-β-lactamase. *Protein Sci.* **12**, 1368–1375
54. Scrofani, S.D.B., Chung, J., Huntley, J.J.A., Benkovic, S.J., Wright, P.E., and Dyson, H.J. (1999) NMR characterization of the metallo-β-lactamase from *Bacteroides fragilis* and its interaction with a tight-binding inhibitor: role of an active-site loop. *Biochemistry* **38**, 14507–14514
55. Salsbury, F.R. Jr, Crowley, M.F., and Brooks, C.L. III. (2001) Modeling of the metallo-β-lactamase from *B. fragilis*: structural and dynamic effects of inhibitor binding. *Proteins: Struct., Funct., Genet.* **44**, 448–459
56. Addison, A.W., Rao, T.N., Reedijk, J., van Rijn, J., and Verschoor, G.C. (1984) Synthesis, structure, and spectroscopic properties of copper(II) compounds containing nitrogen–sulphur donor ligands; the crystal and molecular structure of aqua[1,7-bis(N-methylbenzimidazol-2-yl)-2,6-dithiaheptane]copper(II) perchlorate. *J. Chem. Soc., Dalton Trans.* 1349–1356
57. Ullah, J.H., Walsh, T.R., Taylor, I.A., Emery, D.C., Verma, C.S., Gamblin, S.J., and dand Spencer, J. (1998) The crystal structure of the L1 metallo-

β-lactamase from *Stenotrophomonas maltophilia* at 1.7 Å resolution. *J. Mol. Biol.* **284**, 125–136
58. Wang, Z., Fast, W., Valentine, A.M., and Benkovic, S.J. (1999) Metallo-β-lactamase: Structure and mechanism. *Curr. Opin. Chem. Biol.* **3**, 614–622
59. Tamames, B., Sousa, S.F., Tamames, J., Fernandes, P.A., and Ramos, M.J. (2007) Analysis of zinc-ligand bond lengths in metalloproteins: trends and patterns. *Proteins* **69**, 466–475
60. Rossolini, G.M., Franceschini, N., Riccio, M.L., Mercuri, P.S., Perilli, M., Gaalleni, M., Frère, J.-M., and Amicosante, G. (1998) Characterization and sequence of the *Chryseobacterium* (*Flavobacterium*) *meningosepticum* carbapenemase: a new molecular class B β-lactamase showing a broad substrate profile. *Biochem. J.* **332**, 145–152
61. Orellano, E.G., Girardini, J.E., Cricco, J.A., Ceccarelli, E.A., and Vila, A.J. (1998) Spectroscopic characterization of a binuclear metal site in *Bacillus cereus* β-lactamase II. *Biochemistry* **37**, 10173–10180
62. Davies, R.B. and Abraham, E.P. (1974) Metal cofactor requirements of β-lactamase II. *Biochem. J.* **143**, 129–135
63. Baldwin, G.S., Galdes, A., Hill, H.A., Smith, B.E., Waley, S.G., and Abraham, E.P. (1978) Histidine residues of zinc ligands in β-lactamase II. *Biochem. J.* **175**, 441–447
64. Crowder, M.W., Wang, Z., Franklin, S.L., Zovinka, E.P., and Benkovic, S.J. (1996) Characterization of the metal-binding sites of the β-lactamase from *Bacteroides fragilis*. *Biochemistry* **35**, 12126–12132
65. Laraki, N., Franceschini, N., Rossolini, G.M., Santucci, P., Meunier, C., de Pauw, E., Amicosante, G., Frère, J.M., and Galleni, M. (1999) Biochemical characterization of the *Pseudomonas aeruginosa* 101/1477 metallo-β-lactamase IMP-1 produced by *Escherichia coli*. *Antimicrob. Agents Chemother.* **43**, 902–906
66. Corpet, F. (1988) Multiple sequence alignment with hierarchical clustering. *Nucleic Acids Res.* **16**, 10881–10890

MedChemComm

Dynamic Article Links

Cite this: *Med. Chem. Commun.*, 2011, **2**, 720

www.rsc.org/medchemcomm

CONCISE ARTICLE

Metal preference of Zn(II) and Co(II) for the dinuclear metal binding site of IMP-1 metallo-β-lactamase and spectroscopic properties of Co(II)-substituted IMP-1 with mercaptoacetic acid†

Yoshihiro Yamaguchi,‡*[a] Kayo Imamura,[b] Ako Sasao,[c] Emi Murakami,[b] Yoshichika Arakawa§[d] and Hiromasa Kurosaki‡*[b]

Received 28th February 2011, Accepted 6th May 2011
DOI: 10.1039/c1md00062d

IMP-1 metallo-β-lactamase is a dinuclear Zn(II) enzyme that catalyzes the hydrolysis and inactivation of most β-lactams including carbapenems, and is involved in one of the mechanisms for generating clinical resistance to antibiotics in pathogenic bacteria. We investigated the metal preferences of Zn(II) and Co(II) for the apo-enzyme of IMP-1 metallo-β-lactamase, apo-IMP-1, which contains a dinuclear metal binding site (the Zn1 and Zn2 sites), by UV-visible spectroscopy. The UV-visible spectrum of apo-IMP-1 containing 1 equiv. of Co(II) and 1 equiv. of Zn(II) showed a high preference of Zn(II) for the Zn1 site compared to Co(II). Moreover, Zn(II) bound more strongly to the Zn2 site than Co(II). The interaction of IMP-1 metallo-β-lactamase with mercaptoacetic acid was also investigated using Co(II)-substituted IMP-1 and UV-visible spectroscopy. Possible metal binding modes of Co(II) or Zn(II) to the dinuclear metal binding site in apo-IMP-1 and of mercaptoacetic acid to Co(II)-substituted IMP-1 are proposed.

Introduction

Metallo-β-lactamases are Zn(II)-dependent enzymes that catalyze the hydrolysis of most β-lactams including carbapenems with the exception of monobactams such as aztreonam, and are now recognized as a new potential threat to human society. Some metallo-β-lactamases including IMP-1 discovered in Japan are coded by a gene cassette in an integron and are transferable to other bacteria.[1,2] Since a new metallo-β-lactamase, NDM-1, has just emerged in India and Pakistan, and also been expanding in the United Kingdom[3] and in other countries, further worldwide proliferation of the kind of metallo-β-lactamases is becoming a grave general concern.[4] One countermeasure to these lactamases involves the development of inhibitors that block the action of the enzyme. At present, no relevant inhibitors are available for clinical use. In our continuing efforts to develop metallo-β-lactamase inhibitors, we found that mercaptocarboxylic acids are potent inhibitors for IMP-1.[5] Among them, mercaptoacetic acid and 2-mercaptopropionic acid strongly and competitively inhibited IMP-1 with K_i values of 0.23 and 0.19 μM, respectively.[5]

Based on the inhibition effect of mercaptoacetic acid against IMP-1, Arakawa *et al.* developed a double-disk method for detection of metallo-β-lactamase-producing Gram-negative bacteria.[6] This disk (named SMA disk) is composed of two Kirby–Bauer disks containing ceftazidime and a filter disk containing sodium mercaptoacetate. By changing the shape of the growth inhibitory zone around the disk containing ceftazidime or imipenem, the presence or absence of metallo-β-lactamase-producing bacteria could be judged.

In 2000, the X-ray crystal structure of IMP-1 was determined (Fig. 1).[7] IMP-1 is composed of an αβ/βα fold and two distinct Zn(II) binding sites, which are located at the bottom of a wide shallow groove between the β-sheets. One of the Zn(II) ions, Zn1, is tetrahedrally coordinated by three histidine residues (His116, His118, and His196, according to BBL numbering scheme[8]). Another Zn(II) ion, Zn2, is trigonal-bipyramidally coordinated by Asp120, Cys221, His263, and a water molecule. In addition, the water molecule is bridged to the two Zn(II) ions (presumably,

[a]*Environmental Safety Center, Kumamoto University, 39-1 Kurokami 2-Chome, Kumamoto, 860-8555, Japan. E-mail: yyamagu@gpo.kumamoto-u.ac.jp; Fax: +81 96 342 3237; Tel: +81 96 342 3238*

[b]*Department of Structure–Function Physical Chemistry, Graduate School of Pharmaceutical Sciences, Kumamoto University, 5-1 Oe-honmachi, Kumamoto, 862-0973, Japan. E-mail: ayasaya@gpo.kumamoto-u.ac.jp; Fax: +81 96 371 4314; Tel: +81 96 371 4314*

[c]*Department of Forensic Medicine, Graduate School of Medical Sciences, Kumamoto University, 1-1-1 Honjo, Kumamoto, 860-8556, Japan*

[d]*Department of Bacterial Pathogenesis and Infection Control, National Institute of Infectious Diseases, 4-7-1 Gakuen, Musashi-Murayama, Tokyo, 208-0011, Japan*

† Electronic supplementary information (ESI) available: UV-visible spectral changes of Co(II) with varying concentrations of mercaptoacetic acid (Fig. S1). See DOI: 10.1039/c1md00062d

‡ These authors contributed equally to the work.

§ Present address: *Department of Bacteriology, Nagoya University Graduate School of Medicine, 65 Tsurumai-cho, Showa-ku, Nagoya, Aichi 466-8550, Japan*

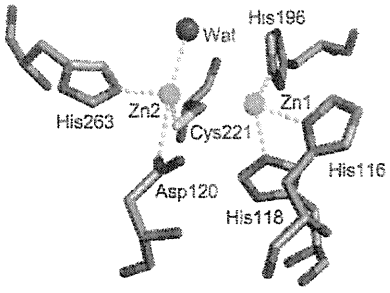

Fig. 1 Schematic representation of the active site of IMP-1 from *Pseudomonas aeruginosa* (PDB code 1DDK). The Zn(II) atoms and a water molecule are shown as spheres.

as a hydroxide ion), although the electron density of this water molecule was not observed in the X-ray crystal structure.

The relationship between the role of each metal ion in the active site and its catalytic activity in metallo-β-lactamases remains controversial. Unfortunately, spectroscopic studies to characterize the metal binding sites have been limited, due to the physicochemical properties of Zn(II). It would be beneficial to exchange Zn(II) with Co(II), which yields a structurally similar and catalytically active analog. One method to prepare Co(II)-substituted enzymes of metallo-β-lactamases is the direct addition of Co(II) to an apo-enzyme that is prepared by the use of chelators and dialysis. The preparation of apo- and Co(II)-substituted enzymes of BcII and CcrA metallo-β-lactamases has been successful.[9–13] Although the preparation of the apo-enzyme of IMP-1 metallo-β-lactamase, apo-IMP-1, has been attempted, complete demetallation with chelators such as EDTA resulted in failure. Very recently, we established a preparation technique for apo-IMP-1 metallo-β-lactamase, which has restored enzyme activity upon addition of Zn(II) ions.[14] Using this technique, we were able to investigate spectroscopic studies on Co(II)-substituted IMP-1.

In this paper, we investigated the metal preferences of Co(II) or Zn(II) for apo-IMP-1 and the spectral properties of mercaptoacetic acid with Co(II)-substituted IMP-1, using UV-visible spectroscopy.

Results and discussion

Metallo-β-lactamases are Zn(II)-dependent enzymes that hydrolyze most β-lactams, even in environments in which the Zn(II) concentration is extremely low. Analysis of the coordination environment around the Zn(II) active site is of great importance for elucidating the relationship between the role of individual Zn (II) ions and the catalytic mechanism of metallo-β-lactamases. Zn (II) ions are, however, "spectroscopically silent" d^{10} metal ions. Therefore, substitution of Zn(II) by Co(II) has become an essential technique to address the structural basis of catalytic properties in Zn(II) enzymes.[15] From this standpoint, the preparation of an apo-enzyme is a crucial step.

For metallo-β-lactamases, apo-enzymes of BcII and CcrA have been prepared and spectroscopic properties of their Co(II)-substituted enzymes were investigated.[9–13] In IMP-1, however, apo-enzymes prepared by the dialysis method were not recovered perfectly after the addition of excess $Zn(NO_3)_2$,[16,17] and the quest for the preparation of an apo-enzyme and metal substitution is ongoing.

Recently, we established a preparation method for apo-IMP-1 with a combination of the chelating agent, EDTA, and a desalting technique with a PD-10 column.[14] As a result, upon addition of Zn(II) ions to the prepared apo-IMP-1, the enzyme activity could be recovered comparable to that observed with the native enzyme. Thus, this preparation allowed us to investigate the spectroscopic properties of Co(II)-substituted IMP-1.

Binding of Co(II) to apo-IMP-1

We previously carried out the spectrophotometric titration of apo-IMP-1 with Co(II) in 50 mM MOPS–NaOH (pH 7.0), 1.0 M NaCl, and 30% glycerol.[14] The UV-visible spectral changes in 50 mM Tris–HCl (pH 7.4), 1.0 M NaCl, and 25% glycerol are shown in Fig. 2A. Note that the spectra were almost identical even when taken in the different buffer solutions. Successive addition of Co(II) to apo-IMP-1 exhibited an intense S^- of Cys221 → Co(II) ligand-to-metal charge transfer (LMCT) band at 350 nm and d–d absorptions in the range of 500–650 nm. The assignment of the LMCT band at 350 nm is supported by disappearance of this band in the UV-visible spectra of the Co(II)-substituted mutants of IMP-1 and other metallo-β-lactamases,[9,11,14] where the Cys221 ligand is replaced by Ala or Ser. Absorbances in both the LMCT and d–d bands continued to increase as Co(II) was added, reaching a plateau at 2 equiv. per apo-IMP-1. The spectrum of apo-IMP-1 containing 1.0 equiv. of Co(II) exhibited absorption maxima at 350, 520, 552, 612, and 635 nm (Fig. 2A). Judging from the increase in the absorbance of the LMCT band at 350 nm, Co(II) distributes between the two sites in the ratio of 2 in the Zn1 site to 1 in the Zn2 site. This result agrees with that for BcII reported by de Seny *et al.*[11] Macroscopic dissociation constants for apo-IMP-1 with Co(II) were derived from spectral changes of the enzyme upon Co(II) binding, using the program DynaFit,[18] and found to be $K_{D1} < 60$ nM and $K_{D2} = 0.3$ μM.[14]

Binding selectivity of Co(II) and Zn(II) to the Zn1 and Zn2 sites in apo-IMP-1

Next, we investigated the preference of Co(II) and Zn(II) for two metal binding sites. Spectral changes of apo-IMP-1 upon successive addition of 1 equiv. of Co(II), followed by the addition of Zn(II) (by 0.2 equiv. increments for each metal) in 50 mM Tris–HCl (pH 7.4), 1.0 M NaCl, and 25% glycerol are shown in Fig. 2B. As described above, the spectrum of apo-IMP-1 containing 1 equiv. of Co(II) exhibited absorption maxima at 350, 520, 552, 612, and 635 nm. Addition of 1 equiv. of Zn(II) to apo-IMP-1 containing 1 equiv. of Co(II) resulted in the increase in the absorbance of the LMCT band at 350 nm, whereas those of the d–d bands in the visible range did not increase significantly with 1 equiv. of Zn(II) added. The increase in the LMCT band at 350 nm is indicative of Co(II) binding at the Zn2 site.[9,11,13,14,19,20] Therefore, this spectral behaviour seems to indicate that Co(II) is pushed out from the Zn1 site with an occupation of Zn(II) at the Zn1 site and shifted to the Zn2 site. This result suggests that Zn (II) preferentially binds to the Zn1 site over the Zn2 site.

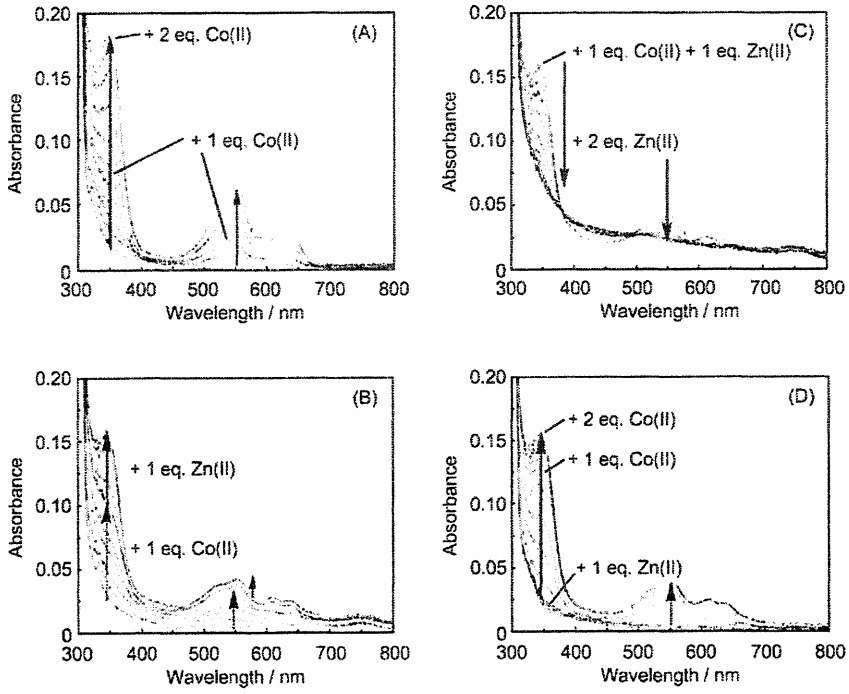

Fig. 2 UV-visible spectral changes of apo-IMP-1 with varying concentrations of Co(II) or Zn(II). (A) Solid arrow: apo-IMP-1 (150 μM) in 50 mM Tris–HCl (pH 7.4), 1.0 M NaCl and 25% glycerol was titrated by 0.2 equiv. of Co(II) to a total of 2 equiv. (B) 1 equiv. of Co(II) in increments of 0.2 equiv. was added to apo-IMP-1 (178 μM) in 50 mM Tris–HCl (pH 7.4), 1.0 M NaCl, and 25% glycerol (dashed arrow), followed by the addition of Zn(II) (0.2 equiv. increments) up to 1 equiv. (solid arrow). (C) 2 equiv. of Zn(II) in increments of 0.2 equiv. was added to apo-IMP-1 containing 1 equiv. of Co(II) and 1 equiv. of Zn(II) (see final spectrum in (B)). (D) 1 equiv. of Zn(II) in increments of 0.2 equiv. was added to apo-IMP-1 (178 μM) in 50 mM Tris–HCl (pH 7.4), 1.0 M NaCl, and 25% glycerol, followed by the addition of Co(II) (0.2 equiv. increment) up to 2 equiv. (solid arrow).

When 2 equiv. of Zn(II) was added to apo-IMP-1 containing 1 equiv. of Co(II) and 1 equiv. of Zn(II), the absorption bands at 350 nm and 500–650 nm disappeared as the concentration of Zn (II) increased (Fig. 2C), suggesting that the replacement of Co(II) by Zn(II) takes place at both the Zn1 and the Zn2 sites, suggesting a higher preference of Zn(II) for both the Zn2 and Zn1 sites than Co(II).

Fig. 2D shows spectral changes of apo-IMP-1 upon successive addition of 1 equiv. of Zn(II), followed by the addition of 2 equiv. of Co(II) (by 0.2 equiv. increment for each metal) in 50 mM Tris–HCl (pH 7.4), 1.0 M NaCl, and 25% glycerol. No change in the spectrum of apo-IMP-1 was observed in the presence of 1 equiv. of Zn(II). The addition of Co(II) resulted in the increase in both the LMCT and d–d bands, where the final spectrum is consistent with that in Fig. 2B, suggesting that Co(II) binds to the Zn2 site. Interestingly, the extinction coefficients (ε) of the LMCT band at 350 nm are *ca.* 730 and *ca.* 900 M^{-1} cm^{-1}, respectively, when 1 and 2 equiv. of Co(II) were added after addition of 1 equiv. of Zn(II) to apo-IMP-1. These values are smaller than that of apo-IMP-1 in the presence of 2 equiv. of Co(II) [Fig. 2A, ε = *ca.* 1200 M^{-1} cm^{-1}, that is, Co(II) totally occupies the Zn2 site], suggesting that Zn(II) was already distributed between the Zn1 and Zn2 sites before addition of Co(II).

Preliminary differential scanning calorimetry measurements also showed enhancement in the denaturation temperature (T_d) from 56.4 °C for apo-IMP-1 or 56.5 °C for mono-Zn(II)-IMP-1 [apo-IMP-1 plus 1 equiv. of Zn(II)] to 76.9 °C for native IMP-1.[14] These analyses revealed that Zn1 contributes to the enzyme activity, whereas Zn2 plays an important role both in stabilizing the protein structure and in increasing catalytic efficiency of the enzyme.

Interaction of mercaptoacetic acid with Co(II)-substituted IMP-1

The coordination of the thiolate group in mercaptoacetic acid to a metal ion in the active site was followed by UV-visible spectroscopy of Co(II)-substituted IMP-1 prepared from apo-IMP-1 and 2 equiv. of Co(II) with mercaptoacetic acid. The spectral changes of Co(II)-substituted IMP-1 with mercaptoacetic acid in 50 mM Tris–HCl (pH 7.4), 1.0 M NaCl, and 25% glycerol are shown in Fig. 3. The addition of mercaptoacetic acid to Co(II)-substituted IMP-1 up to 2 equiv. resulted in a marked increase in the absorbance of the S^--to-Co(II) LMCT band at 350 nm and a shift of the d–d bands (555, 597, and 635 nm) with an increase in the absorbance (Fig. 3). The former feature is characteristic of the S^- of mercaptoacetic acid → Co(II) LMCT band, implicating coordination of the thiolate group of mercaptoacetic acid to Co (II). Bicknell *et al.* prepared Co(II)-substituted angiotensin converting enzyme [Co(II)-ACE] and characterized the catalytic metal binding site both in Co(II)-ACE and in its inhibitor, captopril, by UV-visible spectroscopy.[21] The visible spectrum of Co(II)-ACE exhibits a single broad maximum at 525 nm (ε = 75 M^{-1} cm^{-1}).[21] Upon addition of captopril to Co(II)-ACE, the spectrum of Co(II)-ACE–captopril complex displays peaks at 540 (ε = 350 M^{-1} cm^{-1}), 618 (520), and 637 (560) nm, indicating that maxima at longer wavelength and the increase in the absorbance are changes of the d–d transition of Co(II) by inhibitor binding to the active-site metal. In IMP-1, the spectra of

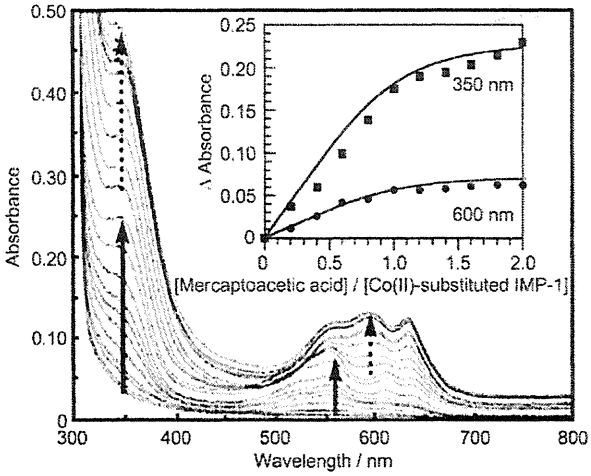

Fig. 3 Spectrophotometric titration of Co(II)-substituted IMP-1 with mercaptoacetic acid. Solid arrow: apo-IMP-1 (171 μM) in 50 mM Tris–HCl (pH 7.4), 1.0 M NaCl, and 25% glycerol was titrated by 0.2 equiv. of Co(II) to a total of 2 equiv. Dashed arrow: 2 equiv. of mercaptoacetic acid in increments of 0.2 equiv. was added to Co(II)-substituted IMP-1 [apo-IMP-1 containing 2 equiv. of Co(II)]. Inset: plot of the absorbances at 350 nm (squares) and 600 nm (circles) as a function of the concentration of added mercaptoacetic acid. The absorbances of apo-IMP-1 and Co(II)-substituted IMP-1 were subtracted from the absorbance of Co(II)-substituted IMP-1 added mercaptoacetic acid. The solid lines represent fits obtained from numerical simulation of a one-step binding model to the data using the program Dynafit (BioKin, Ltd.).[18] The apparent dissociation constant obtained was 14 μM.

Co(II)-substituted IMP-1–mercaptoacetic acid have two features: (i) enhanced absorbance without change in wavelength and (ii) a change in absorption that appears to be a new absorption rather than a shift in an absorption band. This spectral change is similar to that of Co(II)-BcII–D-captopril complex.[22]

When changes in the absorbances at 350 and 650 nm were plotted as a function of the concentration of added mercaptoacetic acid, a plateau was observed for the [mercaptoacetic acid]/[Co(II)-substituted IMP-1] ratio above 1 (Fig. 3, inset), indicating that mercaptoacetic acid binds to Co(II)-substituted IMP-1 to form a 1 : 1 complex. The apparent dissociation constant of mercaptoacetic acid with Co(II)-substituted IMP-1 was estimated by nonlinear least-squares fitting of the spectrophotometric titration data using the program DynaFit,[18] and found to be K_D = 14 μM. In control experiments, it could be ruled out that mercaptoacetic acid binds to a free Co(II) ion because the spectra of $Co(II)SO_4$ in 50 mM Tris–HCl (pH 7.4), 1.0 M NaCl, and 25% glycerol are quite different from those of Co(II)-IMP-1–mercaptoacetic acid complex when mercaptoacetic acid is added from 0 to 2 equiv. (Fig. S1, ESI†).

Antony *et al.* applied the polarizable molecular mechanics method SIBFA to search for the most stable binding modes of captopril and thiomandelate inhibitors to a 104-residue model of CcrA metallo-β-lactamase.[23,24] The most stably bound complex is a monodentate complex, in which S^- bridges the two Zn(II) ions, with the carboxylate and carbonyl groups in captopril or the carboxylate group in thiomandelate interacting with the nearest residues around the dinuclear metal binding site. These

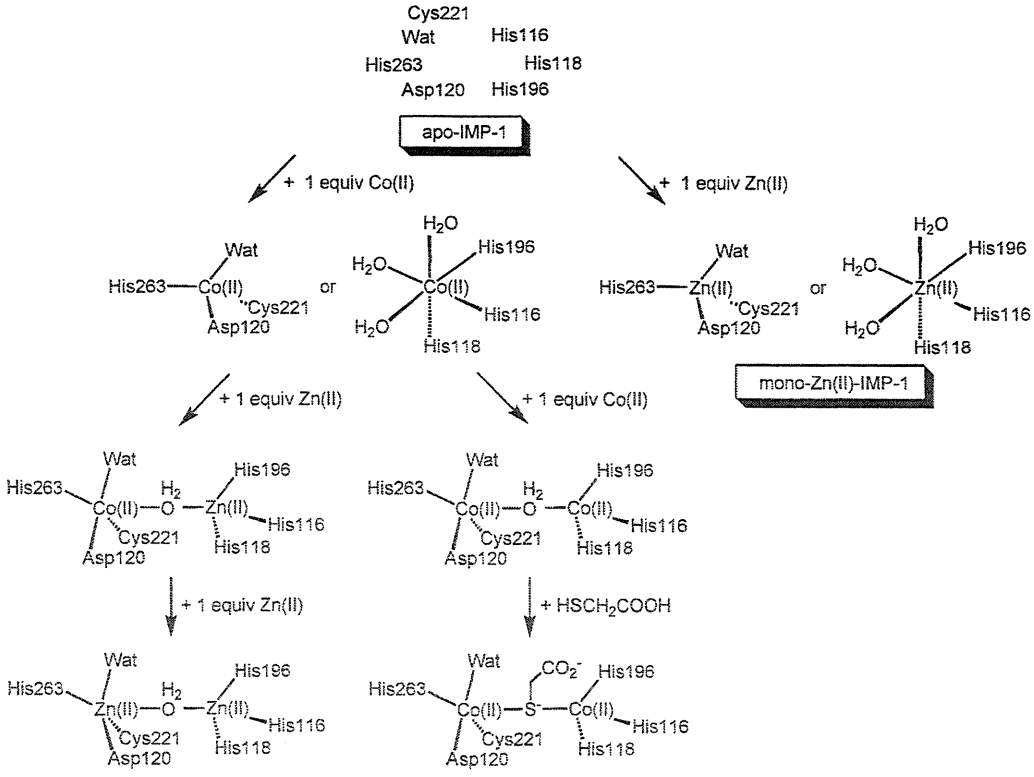

Fig. 4 Proposed modes of reconstruction of IMP-1 from apo-IMP-1 by Zn(II) and Co(II) and the interaction of Co(II)-substituted IMP-1 with mercaptoacetic acid.

are consistent with the X-ray crystal structures of BlaB metallo-β-lactamase complexed with D-captopril[25] and IMP-1 or VIM-2 metallo-β-lactamase complexed with mercaptocarboxylate inhibitors.[7,26]

Considering the results of UV-visible spectroscopy of Co(II)-substituted IMP-1 with mercaptoacetic acid, molecular mechanics calculations, and X-ray crystallography, it was concluded that the thiolate group in mercaptoacetic acid bridges the two Co(II) ions in the active site (Fig. 4).

Conclusions

In summary, we have investigated the metal preference of Co(II) and Zn(II) for dinuclear metal binding sites in apo-IMP-1 and the interaction of Co(II)-substituted IMP-1 with mercaptoacetic acid. We proposed models for the reconstruction of IMP-1 from apo-IMP-1 by Zn(II) and Co(II) and for the interaction of Co(II)-substituted IMP-1 with mercaptoacetic acid (Fig. 4). One equiv. of Co(II) or Zn(II) distributes between both the Zn1 and Zn2 sites. Metal binding modes for Co(II) and Zn(II) to apo-IMP-1 are similar to those found in BcII metallo-β-lactamase.[11,13] Unlike IMP-1 and BcII metallo-β-lactamases, CcrA and Bla2 metallo-β-lactamases showed that Zn(II) binding to apo-enzyme was sequential.[12,19]

Based on the results of UV-visible spectroscopy of Co(II)-substituted IMP-1 with mercaptoacetic acid, the inhibitory effect of mercaptoacetic acid using the double-disk method for detection of metallo-β-lactamase-producing Gram-negative bacteria is thought to arise from the coordination of the thiolate group in mercaptoacetic acid to two Zn(II) ions present in the active site of the metallo-β-lactamase.

Experimental

Chemicals

Antibiotics, cephaloridine from Shionogi & Co., Ltd. (Osaka, Japan) and ampicillin from Meiji Seika Co., Ltd. (Tokyo, Japan), were kindly donated. Cephalothin was purchased from Sigma-Aldrich Co., Ltd. (St Louis, USA). Disodium ethylenediaminetetraacetate (Na_2EDTA), glycerol, and tris(hydroxymethyl)aminomethane (Tris) were purchased from Nacalai Tesque, Inc. (Kyoto, Japan). Mercaptoacetic acid was purchased from Tokyo Chemical Industry Co., Ltd. (Tokyo, Japan). $CoSO_4 \cdot 7H_2O$, ultrapure water, and 3-morpholinopropanesulfonic acid (MOPS) were purchased from Wako Pure Chemical Industries, Ltd. (Osaka, Japan). $Zn(NO_3)_2 \cdot 6H_2O$ was purchased from Katayama Chemical Industries Co., Ltd. (Osaka, Japan). The other reagents were obtained commercially and were of the highest quality available.

Preparation of enzyme

IMP-1 metallo-β-lactamase from *Serratia marcescens* was prepared from the extracts of *Escherichia coli* JM109, which harbored plasmid pSMBNU24 containing the gene, bla_{IMP-1}, of *S. marcescens* TN9106, according to the published method.[5,27] *E. coli* JM109 cells were cultured in the Luria–Bertani medium containing 50 μg mL^{-1} ampicillin at 37 °C for 13 h. The cells were collected by centrifugation (10 000 × *g*) at 4 °C for 15 min and resuspended in 50 mM phosphate buffer (pH 7.0) containing 2 μM $Zn(NO_3)_2$. A crude enzyme solution was obtained from the suspension by sonication followed by centrifugation (150 000 × *g*) at 4 °C for 1 h. IMP-1 was purified by a SP Sepharose Fast Flow column (ϕ 26 mm × 10 cm; flow rate, 60 mL h^{-1}; GE Healthcare UK Ltd., UK) using an eluent of 50 mM phosphate buffer containing 2 μM $Zn(NO_3)_2$ with a gradient of 0 to 0.4 M NaCl in 10 mL fractions and a Sephadex G-75 (ϕ 16 mm × 90 cm; flow rate, 12 mL h^{-1}; GE Healthcare UK Ltd, Buckinghamshire, UK) with 50 mM Tris–HCl buffer (pH 7.4) containing 2 μM Zn $(NO_3)_2$. The fractions (3 mL each) that showed enzymatic activity were collected and concentrated by ultrafiltration (YM-10, Millipore Co., MA, USA). The purity of the enzyme was confirmed by sodium dodecyl sulfate-polyacrylamide gel electrophoresis (SDS-PAGE; PAGEL, SPU-15S, ATTO, Tokyo, Japan) by comparison with protein molecular markers (Oriental Industries Co., Ltd., Tokyo, Japan). The concentration of the purified IMP-1 enzyme was determined by measuring the absorbance at 280 nm of enzyme preparation using an extinction coefficient of 4.9×10^4 M^{-1} cm^{-1}.

β-Lactamase activity

Unless stated otherwise, a spectrophotometric method was used to measure the initial rate of consumption of a substrate, cephalothin or cephaloridine, by the enzyme.

Preparation of apo-IMP-1

Apo-IMP-1 was prepared by a combination of EDTA and desalting column chromatography (PD-10, GE Healthcare UK Ltd., UK) according to our previously reported procedure.[14]

UV-visible spectroscopy. Apo-IMP-1 (150–178 μM) in 50 mM Tris–HCl (pH 7.4), 1.0 M NaCl, and 25% glycerol was titrated by the successive addition of 0.2 equiv. of a $Zn(NO_3)_2$ or $CoSO_4$ stock solution prepared in 50 mM Tris–HCl (pH 7.4), 1.0 M NaCl, and 25% glycerol.

In the spectrophotometric titration of Co(II)-substituted IMP-1 with mercaptoacetic acid, Apo-IMP-1 (171 μM) in 50 mM Tris–HCl (pH 7.4), 1.0 M NaCl, and 25% glycerol was titrated by the sequential addition of 0.2 equiv. of a mercaptoacetic acid stock solution prepared in 50 mM Tris–HCl (pH 7.4), 1.0 M NaCl, and 25% glycerol. UV-visible spectra were recorded at room temperature on a Shimadzu UV-2200 spectrophotometer (Kyoto, Japan), using 1 cm microcells. The interval of each titration was 5 min.

The apparent dissociation constant for mercaptoacetic acid with Co(II)-substituted IMP-1 was derived from spectral changes in absorbances at 350 and 650 nm with increasing concentration of mercaptoacetic acid, using the program DynaFit (BioKin, Ltd.).[18]

The following equilibrium was used for fitting.

$$\text{Co(II)-substituted IMP-1} + \text{mercaptoacetic acid} \overset{K_D}{\rightleftharpoons} \text{Co(II)-substituted IMP-1-mercaptoacetic acid}$$

Acknowledgements

Work related to the preparation and purification of enzyme and UV-visible spectroscopy was supported by the Ministry of

Health, Labor, and Welfare of Japan (grant no. H21-Shinkou-Ippan-008). The DSC measurements were supported in part by a Grant-in-Aid for Scientific Research (B) (no. 183902038) and a Grant-in Aid for Scientific Research (C) (no. 21590116) from the Japanese Society for the Promotion of Science.

References

1 T. R. Walsh, M. A. Toleman, L. Poirel and P. Nordmann, *Clin. Microbiol. Rev.*, 2005, **18**, 306–325.
2 Y. Arakawa, M. Murakami, K. Suzuki, H. Ito, R. Wacharotayankun, S. Ohsuka, N. Kato and M. Ohta, *Antimicrob. Agents Chemother.*, 1995, **39**, 1612–1615.
3 K. K. Kumarasamy, M. A. Toleman, T. R. Walsh, J. Bagaria, F. Butt, R. Balakrishnan, U. Chaudhary, M. Doumith, C. G. Giske, S. Irfan, P. Krishnan, A. V. Kumar, S. Maharjan, S. Mushtaq, T. Noorie, D. L. Paterson, A. Pearson, C. Perry, R. Pike, B. Rao, U. Ray, J. B. Sarma, M. Sharma, E. Sheridan, M. A. Thirunarayan, J. Turton, S. Upadhyay, M. Warner, W. Welfare, D. M. Livermore and N. Woodford, *Lancet Infect. Dis.*, 2010, **10**, 597–602.
4 R. C. Moellering, Jr, *N. Engl. J. Med.*, 2010, **363**, 2377–2379.
5 M. Goto, T. Takahashi, F. Yamashita, A. Koreeda, H. Mori, M. Ohta and Y. Arakawa, *Biol. Pharm. Bull.*, 1997, **20**, 1136–1140.
6 Y. Arakawa, N. Shibata, K. Shibayama, H. Kurokawa, T. Yagi, H. Fujiwara and M. Goto, *J. Clin. Microbiol.*, 2000, **38**, 40–43.
7 N. O. Concha, C. A. Janson, P. Rowling, S. Pearson, C. A. Cheever, B. P. Clarke, C. Lewis, M. Galleni, J.-M. Frère, D. J. Payne, J. H. Bateson and S. S. Abdel-Meguid, *Biochemistry*, 2000, **39**, 4288–4298.
8 M. Galleni, J. Lamotte-Brasseur, G. M. Rossolini, J. Spencer, O. Dideberg, J.-M. Frère and The metallo-β-lactamase working group., *Antimicrob. Agents Chemother.*, 2001, **45**, 660–663.
9 M. W. Crowder, Z. Wang, S. L. Franklin, E. P. Zovinka and S. J. Benkovic, *Biochemistry*, 1996, **35**, 12126–12132.
10 L. I. Llarrull, M. F. Tioni and A. J. Vila, *J. Am. Chem. Soc.*, 2008, **130**, 15842–15851.
11 D. de Seny, U. Heinz, S. Wommer, M. Kiefer, W. Meyer-Klaucke, M. Galleni, J.-M. Frère, R. Bauer and H. W. Adolph, *J. Biol. Chem.*, 2001, **276**, 45065–45078.
12 G. R. Periyannan, A. L. Costello, D. L. Tierney, K. W. Yang, B. Bennett and M. W. Crowder, *Biochemistry*, 2006, **45**, 1313–1320.
13 L. I. Llarrull, M. F. Tioni, J. Kowalski, B. Bennett and A. J. Vila, *J. Biol. Chem.*, 2007, **282**, 30586–30595.
14 Y. Yamaguchi, S. Ding, E. Murakami, K. Imamura, S. Fuchigami, R. Hashiguchi, H. Mori, S. Suzuki, J. Wachino, Y. Arakawa and H. Kurosaki, 2011, submitted.
15 W. Maret and B. L. Vallee, *Methods Enzymol.*, 1993, **226**, 52–71.
16 S. Siemann, D. Brewer, A. J. Clarke, G. I. Dmitrienko, G. Lajoie and T. Viswanatha, *Biochim. Biophys. Acta*, 2002, **1571**, 190–200.
17 S. Haruta, H. Yamaguchi, E. T. Yamamoto, Y. Eriguchi, M. Nukaga, K. O'Hara and T. Sawai, *Antimicrob. Agents Chemother.*, 2000, **44**, 2304–2309.
18 P. Kuzmič, *Anal. Biochem.*, 1996, **237**, 260–273.
19 M. J. Hawk, R. M. Breece, C. E. Hajdin, K. M. Bender, Z. Hu, A. L. Costello, B. Bennett, D. L. Tierney and M. W. Crowder, *J. Am. Chem. Soc.*, 2009, **131**, 10753–10762.
20 E. G. Orellano, J. E. Girardini, J. A. Cricco, E. A. Ceccarelli and A. J. Vila, *Biochemistry*, 1998, **37**, 10173–10180.
21 R. Bicknell, B. Holmquist, F. S. Lee, M. T. Martin and J. F. Riordan, *Biochemistry*, 1987, **26**, 7291–7297.
22 U. Heinz, R. Bauer, S. Wommer, W. Meyer-Klaucke, C. Papamichaels, J. Bateson and H. W. Adolph, *J. Biol. Chem.*, 2003, **278**, 20659–20666.
23 J. Antony, J. P. Piquemal and N. Gresh, *J. Comput. Chem.*, 2005, **26**, 1131–1147.
24 J. Antony, N. Gresh, L. Olsen, L. Hemmingsen, C. J. Schofield and R. Bauer, *J. Comput. Chem.*, 2002, **23**, 1281–1296.
25 I. García-Sáez, J. Hopkins, C. Papamicael, N. Franceschini, G. Amicosante, G. M. Rossolini, M. Galleni, J.-M. Frère and O. Dideberg, *J. Biol. Chem.*, 2003, **278**, 23868–23873.
26 Y. Yamaguchi, W. Jin, K. Matsunaga, S. Ikemizu, Y. Yamagata, J. Wachino, N. Shibata, Y. Arakawa and H. Kurosaki, *J. Med. Chem.*, 2007, **50**, 6647–6653.
27 E. Osano, Y. Arakawa, R. Wacharotayankun, M. Ohta, T. Horii, H. Ito, F. Yoshimura and N. Kato, *Antimicrob. Agents Chemother.*, 1994, **38**, 71–78.

DOI: 10.1002/cbic.201100342

A Demetallation Method for IMP-1 Metallo-β-Lactamase with Restored Enzymatic Activity Upon Addition of Metal Ion(s)

Yoshihiro Yamaguchi,*[a] Shijia Ding,[b] Emi Murakami,[c] Kayo Imamura,[c] Sachiko Fuchigami,[c] Ryo Hashiguchi,[c] Katsuhide Yutani,[d] Hiromasa Mori,[c] Shinnichiro Suzuki,[e] Yoshichika Arakawa,[f] and Hiromasa Kurosaki*[c]

Metallo-β-lactamases (MBLs) are Zn^{II}-dependent enzymes that hydrolyze most β-lactams[1] and pose a potential threat in clinical environments due to their wide substrate specificity and lack of clinically available inhibitors.[2] MBLs are classified into three subclasses, B1, B2, and B3, according to the set of metal ion ligands in the active center.[3] Most recently, a new metallo-β-lactamase has been found in India, Pakistan, and also in the United Kingdom[4] and many other countries. Further proliferation of the types of metallo-β-lactamases is becoming a grave worldwide public health concern.[5] Among the currently known MBLs, IMP-1, belonging to subclass B1, is one of the most serious threats because the gene encoding it is located in an integron structure on a plasmid,[6] which is horizontally transferable between bacterial strains.

The X-ray crystal structure of IMP-1 has been determined and two Zn^{II} ions (termed Zn1 and Zn2) were found in the active center.[7] Zn1 is tetrahedrally coordinated by His116, His118, and His196, whereas Zn2 is trigonal–pyramidally coordinated by Asp120, Cys221, His263, and a water molecule (Figure 1). In addition, OH_2 or OH^- is thought to be bridged between Zn1 and Zn2, although no electron density for this molecule is observed due to the low resolution of the crystal structure.

Correlation between Zn^{II} content and catalytic efficiency continues to be of great controversy,[8] despite the fact that Zn^{II} ligands are well-conserved in other subclass B1 MBLs, for example, BcII from *Bacillus cereus* and CcrA from *Bacteroides fragilis*.[9] BcII has one Zn^{II} ion under physiological conditions but achieves maximum activity when two Zn^{II} ions are bound to the active center. Unlike BcII, CcrA and IMP-1 contain two Zn^{II} ions under physiological conditions and require two Zn^{II} ions for catalysis.

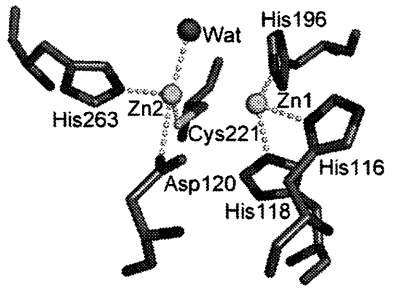

Figure 1. Schematic representation of the active site of IMP-1 from *Pseudomonas aeruginosa* (PDB ID: 1DDK). The Zn^{II} (Zn1, Zn2) atoms and a water (Wat) molecule are shown as spheres.

To investigate the metal coordination environment in the active center, spectroscopic studies on Co^{II}-substituted MBLs have been extensively carried out, due to the spectroscopically silent Zn^{II}.[10] Success in these studies requires preparation of apo-enzymes. In BcII and CcrA, demetallations of Zn^{II} and metal substitution with Co^{II} have been performed successfully.[10] Similar efforts have been attempted for IMP-1, but complete demetallation with various chelating agents, such as EDTA, yields samples that cannot be reactivated in the presence of excess Zn^{II} ions.[11]

Herein, we describe the kinetic behavior of the inactivation of IMP-1 by EDTA, and successful preparation of the apo-enzyme (apo-IMP-1). In addition, spectroscopic characterization of Co^{II}-substituted IMP-1 derived from apo-IMP-1 with Co^{II}, in situ, is also described.

Temperature dependency for inactivation of IMP-1 (10 μM) by EDTA (50 mM) in MOPS (50 mM; pH 7.0) and NaCl (1.0 M) was examined by changing the temperature of the incubation samples (0, 10, 20, and 30 °C, Figure S1 in the Supporting Information). Figure 2 shows the plot of the residual activity against incubation time at 10 °C, where the residual activity, k_t/k_0, (i.e., the relative activity) is the ratio of the molecular activity, k_t, of the activated IMP-1 at each incubation time of IMP-1 with EDTA to the molecular activity, k_0, of IMP-1 before the addition of EDTA at $t=0$ (control).

From Figure 2, it is apparent that the inactivation reaction proceeds in two steps, namely fast and slow. A plausible explanation for this biphasic behavior is successive demetallation of the two Zn^{II} ions from the active center (Scheme 1).

[a] *Prof. Dr. Y. Yamaguchi*
Environmental Safety Center, Kumamoto University
39-1 Kurokami 2-Chome, Kumamoto 860-8555 (Japan)
E-mail: yyamagu@gpo.kumamoto-u.ac.jp

[b] *Prof. Dr. S. Ding*
Department of Medical Laboratory
Chongqing University of Medical Sciences, Chongqing 400016 (China)

[c] *E. Murakami, K. Imamura, S. Fuchigami, R. Hashiguchi, Dr. H. Mori, Prof. Dr. H. Kurosaki*
Department of Structure–Function Physical Chemistry
Graduate School of Pharmaceutical Sciences, Kumamoto University
5-1 Oe-honmcahi, Kumamoto 862-0973 (Japan)
E-mail: ayasaya@gpo.kumamoto-u.ac.jp

[d] *Prof. Dr. K. Yutani*
RIKEN SPring-8 Center, Harima Institute
1-1-1 Kouto, Sayo, Hyogo 679-5148 (Japan)

[e] *Prof. Dr. S. Suzuki*
Department of Chemistry, Graduate School of Science
Osaka University, Toyonaka, Osaka 560-0043 (Japan)

[f] *Prof. Dr. Y. Arakawa*
Department of Bacteriology
Nagoya University Graduate School of Medicine
65 Tsurumai-cho, Showa-ku, Nagoya, Aichi 466-8550 (Japan)

Supporting information for this article is available on the WWW under http://dx.doi.org/10.1002/cbic.201100342.

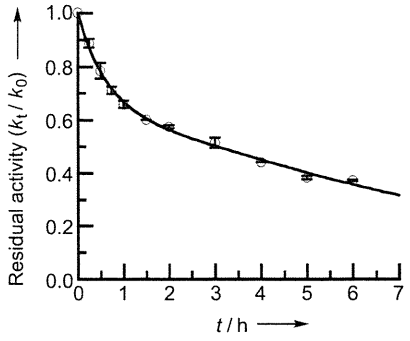

Figure 2. Residual activity of IMP-1 (10 μM) against time in MOPS-NaOH (50 mM, pH 7.0) and NaCl (1.0 M) at 10 °C in the presence of EDTA (50 mM). Values are the mean ± S.D. from three independent experiments performed in duplicate. The solid line was generated by a nonlinear least-squares fit of the data to Equation (1), as described in the text.

$$\text{di-Zn}^{II}\text{-IMP-1 + EDTA} \xrightarrow{k_f} \text{mono-Zn}^{II}\text{-IMP-1 + Zn}^{II}\text{-EDTA}$$

$$\text{mono-Zn}^{II}\text{-IMP-1 + EDTA} \xrightarrow{k_s} \text{apo-IMP-1 + Zn}^{II}\text{-EDTA}$$

Scheme 1. Successive demetallation of the two Zn^{II} ions from the active center of IMP-1.

Assuming that the kinetics of demetallation from IMP-1 obey two pseudo-first-order reactions (Equations (S1)–(S6) in the Supporting Information), the residual activity can be expressed by Equation (1), where k_f and k_s are the rate constants for the fast and slow inactivation reactions, respectively:

$$\frac{k_t}{k_0} = \exp(-k_f t) + \frac{k_f}{k_s - k_f}[\exp(-k_f t) - \exp(-k_s t)] \times \alpha \qquad (1)$$

We estimated the following rate constants and α for inactivation of IMP-1 with EDTA at 10 °C using a nonlinear least-squares fitting of the experimental data to Equation (1): $k_f = 1.26(\pm 0.06)\ h^{-1}$, $k_s = 0.12(\pm 0.01)\ h^{-1}$, and $\alpha = 0.67 \pm 0.04$. At temperatures other than 0 °C, however, the transition from the faster phase to the slower phase could not clearly be discriminated (Figure S1 in the Supporting Information).

Inactivation of IMP-1 with EDTA is a complicated process. Laraki et al. have suggested that the inactivation of IMP-1 by a metal ion chelator follows a pseudo-first-order reaction and have proposed the mechanism shown in Scheme 2, where E*–Zn^{II}–C represents the inactive ternary complex of the enzyme–Zn^{II}–chelator.[12] They found that EDTA is a poor inactivator because only 10% of the activity was lost after 1 h with 10 mM chelator in HEPES (50 mM, pH 7.5).[12] Siemann et al. also described the inactivation of IMP-1 with chelators based on Scheme 2, but the inactivation was not reversible except in the case of one chelator (zincon).[11b] The treatment of IMP-1 with dipicolinic acid resulted in production of the mono-Zn^{II}–IMP-1, as determined by electrospray ionization mass spectrometry under nondenaturing conditions. The k_{cat} value of mono-Zn^{II}–IMP-1 (137 s^{-1}) for nitrocefin as the substrate was approximately half that of di-Zn^{II}–IMP-1 (260 s^{-1}); this indicates that the second equivalent of Zn^{II} enhances enzyme catalytic activity.[11b]

$$\text{E–Zn}^{II} + \text{C} \underset{}{\overset{K_I}{\rightleftharpoons}} \text{E–Zn}^{II}\text{–C} \xrightarrow{k_{inact}} \text{E + Zn}^{II}\text{–C or E*–Zn}^{II}\text{–C}$$

Scheme 2. The mechanism for the inactivation of IMP-1 by a metal ion chelator according to the proposed pseudo-first-order reaction.[12] E*–Zn^{II}–C is the inactive ternary complex of the enzyme–Zn^{II}–chelator.

In this study, the relative ratio of the activity of mono-Zn^{II}–IMP-1 to that of di-Zn^{II}–IMP-1, α, was found to be 0.67. This indicates that the activity of mono-Zn^{II}–IMP-1 is 67% that of the parent di-Zn^{II}–IMP-1 and that the two Zn^{II} ions have different binding affinities for IMP-1. Based on the results described above, we attempted to prepare apo-IMP-1 by the application of relatively high temperature and high enzyme concentration (see the Supporting Information). A typical procedure is as follows. A solution of EDTA (200 mM) in MOPS-NaOH (50 mM, pH 6.5) and NaCl (1.0 M) was added drop-wise to the slowly stirred IMP-1 solution (1.5 mM) in MOPS-NaOH (50 mM, pH 6.5), NaCl (1.0 M), and glycerol (30%). The final concentration of EDTA was adjusted to 50 mM. After incubation at 30 °C and centrifugation, the supernatant was passed through a PD-10 column at 4 °C. This method yielded preparations with 0.025 Zn^{II} per molecule of IMP-1, as checked by atomic absorption spectrometry, and the activity of apo-IMP-1 was less than 5% that of native IMP-1. The addition of excess $Zn(NO_3)_2$ to apo-IMP-1 showed activity comparable to that of the native enzyme (Table S1 in the Supporting Information). When 2 equiv Zn^{II} was added to apo-IMP-1, the CD spectrum of reconstituted IMP-1 was consistent with that of native IMP-1 (Figure 3A); this indicates that the helix content does not change and the secondary structure in the protein is maintained.

Preliminary differential scanning calorimetry measurements also showed an increase of the denaturation temperature from 56.4 °C for apo-IMP-1 or 56.5 °C for mono-Zn^{II}–IMP-1 (apo-IMP-1 + 1 equiv Zn^{II}) to 76.9 °C for native IMP-1 (Figure 3B). These findings suggest that the second equivalent of Zn^{II} contributes both to enhance catalytic activity and structural stability in the Zn^{II} coordination sphere during the catalytic cycle, which can help to achieve maximum activity.

In contrast, the preparation of apo-IMP-1 by a dialysis method with EDTA at 4 °C took about 143 h, and was unsuccessful due to irreversible denaturation. Haruta et al. also reported the preparation of apo-IMP-1 by three days of dialysis of the EDTA-treated enzyme against Zn^{II}-free MOPS, but only 30% of its original activity was restored, even after addition of 1 mM $Zn(NO_3)_2$ to apo-IMP-1.[11a]

To extrapolate the coordination environment of mono-Zn^{II}– and di-Zn^{II}–IMP-1, spectrophotometric titration of prepared apo-IMP-1 with $CoCl_2$ was carried out in MOPS-NaOH (50 mM, pH 7.0), NaCl (1.0 M), and glycerol (30%) under argon. Figure 4A shows the UV-visible difference spectral changes when $CoCl_2$ was added, up to 2 equiv in 0.2 equiv increments (the spectrum of apo-IMP-1 was subtracted from each spectrum of

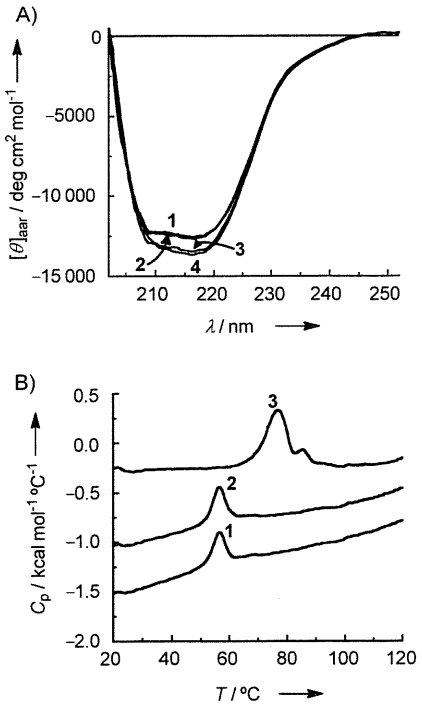

Figure 3. A) CD spectra of apo-IMP-1 (**1**), mono-Zn^{II}–IMP-1 (**2**; apo-IMP-1 + 1 equiv Zn^{II}), native IMP-1 (**3**), and di-Zn^{II}–IMP-1 (**4**; apo-IMP-1 + 2 equiv Zn^{II}) in MOPS-NaOH (50 mM, pH 7.0), NaCl (1.0 M), and glycerol (30%) at 25 °C, and B) DSC transitions of apo-IMP-1 (**1**; 34 μM), mono-Zn^{II}–IMP-1 (**2**; apo-IMP-1 + 1 equiv Zn^{II}; 38 μM), and native IMP-1 (**3**; 36 μM) in potassium phosphate (50 mM, pH 7.0), NaCl (1.0 M), and glycerol (30%).

the Co^{II} added enzyme). For concentrations up to 1 equiv of Co^{II}, an intense absorption band was observed at 350 nm, which was attributed to the thiolate group of Cys221→Co^{II} ligand-to-metal charge transfer (LMCT) band. Concurrently, d–d transitions in the range of 500–650 nm were also observed. Further addition of 1 equiv Co^{II} to mono-Co^{II}–IMP-1 gave the LMCT band at 350 nm (difference molar extinction coefficient, $\varepsilon = 1200\ M^{-1}cm^{-1}$) and four readily distinguishable d–d transitions at 520 (280), 556 (360), 612 (250), and 635 nm (210).

The molar extinction coefficient increased with increasing concentration of Co^{II} and reached a plateau when the Co^{II} content exceeded 2 equiv (Figure 4A, inset), but preferential absorption at either 350 or 500–650 nm was not observed. The molar extinction coefficient at 350 nm in di-Co^{II}–IMP-1 is about threefold higher than that in mono-Co^{II}–IMP-1. Although more accurate estimation of the dissociation constants by competition experiments with chelators, such as Mag-fura-2, could be performed, the macroscopic dissociation constants were estimated by fitting of the titration data by using the program DynaFit,[13] and found to be $K_{D1} < 60$ nM and $K_{D2} = 0.3$ μM (Figure 4A, inset, and Table S2 in the Supporting Information), which are close to those of BcII (Table S2 in the Supporting Information). No precipitation was observed even up to the addition of 3 equiv of $CoCl_2$ to apo-IMP-1. In contrast, de Seny et al. and Periyannan et al. reported that the addition of Co^{II} to apo-BcII and apo-CcrA resulted in the formation of a precipitate.[10b,d]

Assignment of the coordination geometries by absorption and CD spectra have proven difficult for Co^{II} complexes and Co^{II}-substituted metalloenzymes. The room temperature magnetic circular dichroism (MCD) spectra in conjunction with absorption spectra provide valuable information in defining the overall coordination geometries of Co^{II} coordination sites more accurately.[14] The room temperature MCD spectra of apo-IMP-1 containing 1.0 and 2.0 equiv Co^{II} in MOPS-NaOH (50 mM, pH 7.0), NaCl (1.0 M), and glycerol (30%) are shown in Figure 4C. The addition of 1.0 equiv of Co^{II} to apo-IMP-1 resulted in two extrema at 330(−) nm and 360(+) nm, derived from a Cys221→Co^{II} LMCT band, and a broad negative extrema near 550 nm. The addition of 2 equiv of Co^{II} to apo-IMP-1 gave rise to six distinct extrema at 335(−), 360(+), 520(+), 556(−), 612(−), and 635(−) nm, with a substantial increase in the intensity, which is quite similar to that of the pentacoordinate Co^{II}-substituted β-lactamase II.[10h]

For detailed examination of the Co^{II} coordination sphere in Co^{II}-substituted IMP-1, the C221A mutant in which cysteine at position 221 is replaced by alanine was over-expressed and purified. This apo-enzyme (apo-C221A) was then prepared according to our procedure described above (see the Supporting Information).

The UV/Vis difference spectrum (Co^{II}-bound apo-C221A) of apo-C221A containing 1 equiv Co^{II} in MOPS-NaOH (50 mM, pH 7.0), NaCl (1 M), and glycerol (30%) exhibited an absorption maximum at 550 nm ($\varepsilon = 130\ M^{-1}cm^{-1}$, Figure 4B). The macroscopic dissociation constant was estimated by fitting of the titration data, and found to be $K_{D1} = 2.4$ μM (Figure 4B, inset, and Table S2 in the Supporting Information). The corresponding MCD spectrum showed an intense negative extremum between 500 and 600 nm (Figure 4D). This MCD spectrum is analogous to those of tetrahedral Co^{II} enzymes, such as the acidic form of carbonic anhydrase;[14] this indicates that Co^{II} in mono-Co^{II}–C221A is likely to occupy the Zn1 site with tetracoordinate Co^{II} geometry. No LMCT band from Cys221→Co^{II} was observed. Further addition of 1 equiv of Co^{II} to mono-Co^{II}–C221A resulted in a spectral change with a similar shape. From a comparison of the UV/Vis difference and MCD spectra between IMP-1 and the C221A mutant, the d–d transitions in the range of 500–600 nm are mainly due to metal binding at the Zn1 site, but those at 612 and 635 nm are partially attributed to metal binding at the Zn2 site. Moreover, the results of our spectroscopic data suggest that Co^{II} in mono-Co^{II}–IMP-1 might be distributed between both the Zn1 and Zn2 sites with a ratio of about 2:1. These results are supported by the prediction for BcII by de Seny et al.,[10b] in which the metal ion is distributed between both sites when the apo-enzyme is reconstituted with 1 equiv of Co^{II} or Cd^{II}.

In conclusion, we have established a new preparation method for generating the apo-enzyme of IMP-1, in which the activity can be restored by the addition of Zn^{II} ions. Key to the successful preparation of apo-IMP-1 are: 1) inclusion of 1.0 M NaCl and more than 10% glycerol in buffer, 2) demetallation for a short time (~12 h) at mild temperature (30 °C) without di-

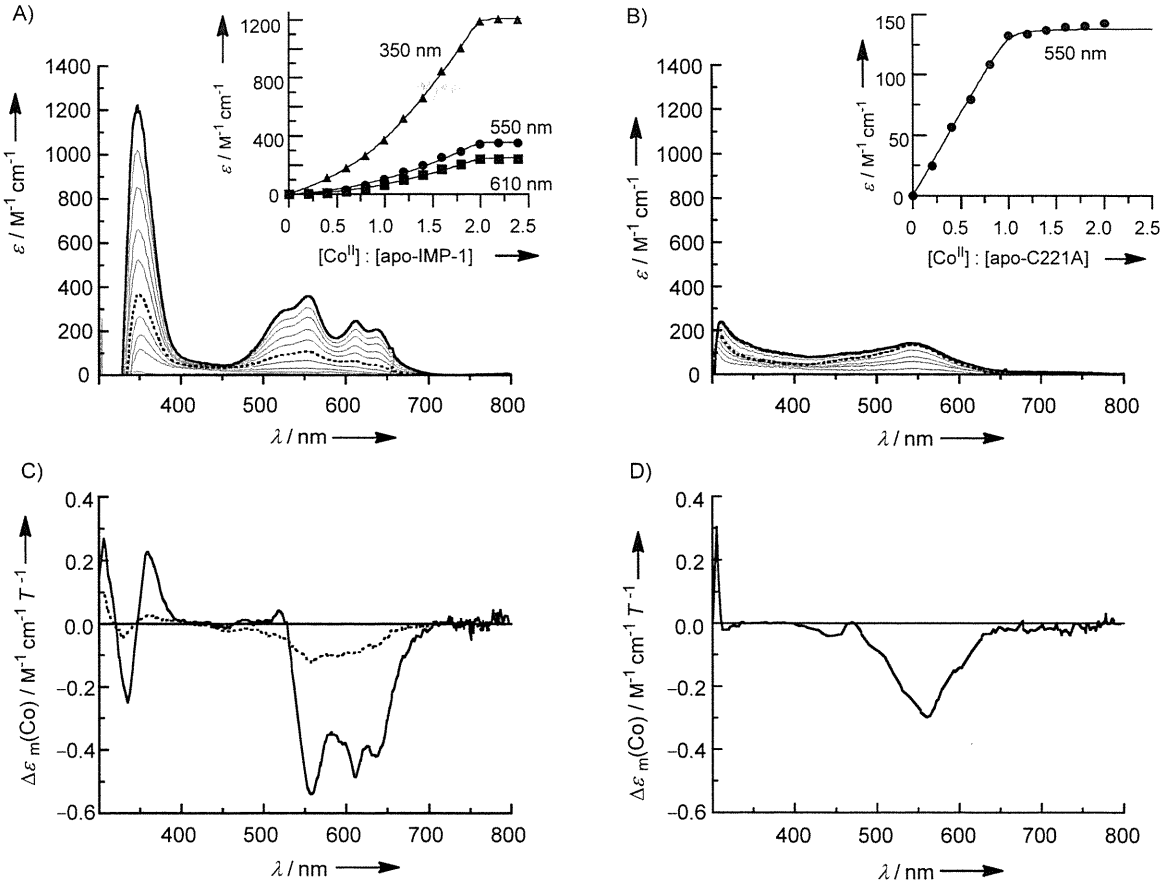

Figure 4. UV–visible difference and MCD spectra of apo-IMP-1 and apo-C221A with Co^{II}. A) apo-IMP-1 (633 μM) in MOPS-NaOH (50 mM, pH 7.0), NaCl (1.0 M), and glycerol (30%) was titrated with 0.2, 0.4, 0.6, 0.8, 1.0, 1.2, 1.4, 1.6, 1.8, and 2.0 equiv of Co^{II}. The thick broken and solid lines show the addition of Co^{II} to apo-IMP-1 up to 1 and 2 equiv, respectively. The spectrum of apo-IMP-1 was subtracted from each spectrum of the Co^{II}-added enzyme. Inset: plot of the difference molar extinction coefficient (ε) at 350, 550, and 610 nm as a function of Co^{II} equivalents added to apo-IMP-1. The solid lines correspond to a sequential two-step binding model (see the Supporting Information) by using the program DynaFit (BioKin, Ltd.).[13] The dissociation constants obtained were $K_{D1} <$ 60 nM and $K_{D2} = 0.3$ μM. B) apo-C221A (516 μM) in MOPS-NaOH (50 mM, pH 7.0), NaCl (1.0 M), and glycerol (30%) was titrated with 0.2, 0.4, 0.6, 0.8, 1.0, 1.2, 1.4, 1.6, 1.8, and 2.0 equiv of Co^{II}. The thick broken and solid lines show the addition of Co^{II} to apo-C221A up to 1 and 2 equiv, respectively. The spectrum of apo-C221A was subtracted from each spectrum of the Co^{II}-added enzyme. Inset: plot of the difference molar extinction coefficient (ε) at 550 nm as a function of Co^{II} equivalents added to apo-C221A. The solid line corresponds to a one-step binding model (see the Supporting Information) by using the program DynaFit.[13] The dissociation constant obtained was $K_{D1} = 2.4$ μM. C) The room temperature MCD spectra of apo-IMP-1 (510 μM) upon the addition of 1 equiv (-----) and 2 equiv (——) Co^{II} in MOPS-NaOH (50 mM, pH 7.0), NaCl (1.0 M), and glycerol (30%). D) The room temperature MCD spectra of apo-C221A (650 μM) upon addition of 2 equiv Co^{II} in MOPS-NaOH (50 mM, pH 7.0), NaCl (1.0 M), and glycerol (30%).

alysis, and 3) choice of desalting column. Based on the success of this apo-enzyme preparation, the spectroscopic properties of apo-IMP-1 with Co^{II} ions could then be investigated. Finally, this method can be used to prepare not only apo-IMP-1, but also other metallo-β-lactamases. Indeed, the apo-enzyme of IND-7 metallo-β-lactamase could be prepared easily.

Acknowledgements

Work related to the preparation and purification of native- and apo-enzymes of IMP-1 was supported by a grant from the Ministry of Health, Labor, and Welfare of Japan (H21-Shinkou-Ippan-008). The spectroscopic studies were supported in part by the Japanese Society for the Promotion of Science in the form of a Grant-in-Aid for Scientific Research (B) (No. 183902038) and a Grant-in-Aid for Scientific Research (C) (No. 21590116). We thank Dr. Alejandro Vila, Dr. Mariana Tioni, and Dr. Leticia Llarrul for providing the script file of the DynaFit program.

Keywords: antibiotics · bioinorganic chemistry · lactams · metalloenzymes · UV/Vis spectroscopy

[1] K. Bush, G. A. Jacoby, A. A. Medeiros, *Antimicrob. Agents Chemother.* **1995**, *39*, 1211.
[2] a) T. R. Walsh, M. A. Toleman, L. Poirel, P. Nordmann, *Clin. Microbiol. Rev.* **2005**, *18*, 306; b) J. H. Toney, J. G. Moloughney, *Curr. Opin. Investig. Drugs* **2004**, *5*, 823; c) C. Bebrone, *Biochem. Pharmacol.* **2007**, *74*, 1686; d) M. W. Crowder, J. Spencer, A. J. Vila, *Acc. Chem. Res.* **2006**, *39*, 721.
[3] a) "The metallo-β-lactamase working group": M. Galleni, J. Lamotte-Brasseur, G. M. Rossolini, J. Spencer, O. Dideberg, J.-M. Frère, *Antimicrob. Agents Chemother.* **2001**, *45*, 660; b) G. Garau, I. García-Sáez, C. Bebrone, C. Anne, P. Mercuri, M. Galleni, J.-M. Frère, O. Dideberg, *Antimicrob. Agents Chemother.* **2004**, *48*, 2347.
[4] K. K. Kumarasamy, M. A. Toleman, T. R. Walsh, J. Bagaria, F. Butt, R. Balakrishnan, U. Chaudhary, M. Doumith, C. G. Giske, S. Irfan, P. Krishnan, A. V.

